JACS
JOURNAL OF THE AMERICAN CHEMICAL SOCIETY
pubs.acs.org/JACS
Article

Three-Center M−H−B Bonds Are Strong Field Interactions. Synthesis and Characterization of $M(CH_2NMe_2BH_3)_3$ Complexes of Titanium, Chromium, and Cobalt

R. Joseph Lastowski, Jonathan T. Yarranton, Lingyang Zhu, Konstantinos D. Vogiatzis, and Gregory S. Girolami*

Cite This: J. Am. Chem. Soc. 2023, 145, 23585−23599
Read Online
ACCESS | Metrics & More | Article Recommendations | Supporting Information

ABSTRACT: We describe new compounds of stoichiometry $M(CH_2NMe_2BH_3)_3$ (M = Ti, Cr, and Co), each of which contains three chelating boranatodimethylaminomethyl (BDAM) ligands. In all three compounds, the BDAM anion, which is isoelectronic and isostructural with the neopentyl group, is bound to the metal center at one end by a metal−carbon σ bond and at the other by one three-center M−H−B interaction. The crystal structures show that the d^1 titanium(III) compound is trigonal prismatic (or eight-coordinate, if two longer-ranged M···H interactions with the BH_3 groups are included), whereas the d^3 chromium(III) compound and the d^6 cobalt(III) compounds are both *fac*-octahedral. The Cr and Co compounds exhibit two rapid dynamic processes in solution: exchange between the Δ and Λ enantiomers and exchange of the terminal and bridging hydrogen atoms on boron. For the Co complex, the barrier for Δ/Λ exchange ($\Delta G^{\ddagger}_{298}$ = 10.1 kcal mol^{-1}) is significantly smaller than those seen in other octahedral cobalt(III) compounds; DFT calculations suggest that Bailar twist and dissociative pathways for Δ/Λ exchange are both possible mechanisms. The UV−vis absorption spectra of the cobalt(III) and chromium(III) species show that the ligand field splittings Δ_o caused by the M−H−B interactions are unexpectedly large, thus placing them high on the spectrochemical series (near ammonia and alkyl groups); their nephelauxetic effect is also large. The DFT calculations suggest that these properties of M−H−B interactions are in part a consequence of their three-center nature, which delocalizes electron density away from the metal center and reduces electron−electron repulsions.

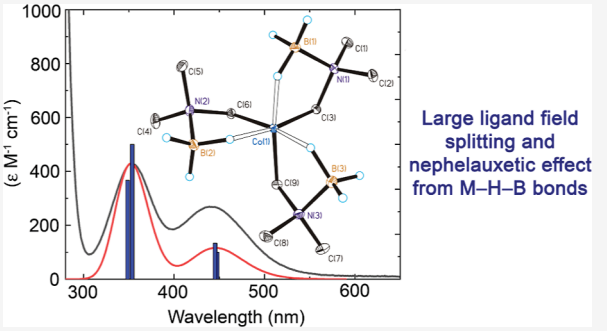

INTRODUCTION

Metal compounds containing borohydride (BH_4^-) ligands have been the focus of much research[1−4] owing to their applications or potential applications in catalysis,[5−8] microelectronics,[9] and energy storage.[4,10] Although borohydride compounds are known for almost all of the transition elements, they remain relatively scarce for metals late in the transition series, in part because these metals are relatively easily reduced and the borohydride anion is a reasonably strong reductant. Essentially, all known late transition metal borohydride compounds contain ancillary ligands (especially carbon monoxide, phosphines, and olefins) that stabilize the metals with respect to reduction to the zerovalent state. Among these late transition metal borohydride compounds are some in which the borohydride groups are incorporated into chelating ligands of the type L-BH_3 (often, L is attached to the borohydride unit by means of some intervening atoms), where L is a Lewis base such as a phosphine,[11−14] chalcogen,[15−18] carbene,[15] pyrazole,[19,20] or amide group.[21]

Relatively little is known about the ligand field properties of borohydride ligands. Borohydrides are known to interact with metals exclusively as σ-type donors,[22,23] but the donor ability of the B−H bond relative to other kinds of (more classical) Lewis bases remains unclear. M−H−B bonds have sometimes been alluded to as strong interactions[16,24,25] and sometimes as weak interactions.[13,17,21,26,27]

Here, we describe the synthesis and characterization of new organometallic borohydride compounds of stoichiometry $M(CH_2NMe_2BH_3)_3$, where M = Ti, Cr, or Co. The boranatodimethylaminomethyl (BDAM) ligand is isoelectronic with the neopentyl anion, but unlike neopentyl (which is invariably a unidentate ligand),[28,29] the BDAM group can readily bind to a metal center in a bidentate fashion: at one end through an sp^3-hybridized alkyl donor and at the other through

Received: July 10, 2023
Published: October 18, 2023

https://doi.org/10.1021/jacs.3c07336
J. Am. Chem. Soc. 2023, 145, 23585−23599

a BH_3 group, the hydrogen atoms of which bear a partial negative charge owing to the electronegativity difference between B and H. The $M(BDAM)_3$ compounds of Co and Cr are octahedral tris(chelate) complexes, and investigations of their dynamic behavior and spectroscopic features, combined with computational studies, have enabled us to compare the ligand field properties of the M−H−B bond with those of more classical Lewis bases. Somewhat surprisingly, we find that the B−H group is a strong field ligand, comparable with ammonia and alkyl groups, and thus remarkably high on the spectrochemical series.

RESULTS AND DISCUSSION

Synthesis and Characterization of $M(BDAM)_3$ Compounds. In 2002, Peters reported that trimethylamine-borane can be deprotonated with *n*-butyllithium in tetrahydrofuran to afford (boranatodimethylaminomethyl)lithium, Li-($CH_2NMe_2BH_3$)·thf (**1**).[30] Although air- and moisture-sensitive, this reagent can be prepared on a large scale (10 g) and stored at room temperature. It is soluble in organic solvents, including diethyl ether, thf, benzene, and toluene.

We find that treatment of $TiCl_4$ with 4 equiv of **1** in diethyl ether at −78 °C results in a blue solution, from which blue prisms can be isolated by crystallization from pentane (Scheme 1). This titanium(III) complex, $Ti(BDAM)_3$ (**2**), where BDAM = boranatodimethylaminomethyl, is sensitive to air and moisture and is also thermally sensitive; it must be kept at 0 °C during manipulations to minimize decomposition. The reduction of Ti^{4+} to Ti^{3+} probably involves reductive elimination of H_2 from a titanium(IV) hydride intermediate; this same reduction is also effected by BH_4^-.[31,32] Interestingly, we have been unable to prepare **2** by treating $TiCl_3(thf)_3$ with 3 equiv of **1**.

Scheme 1. Synthesis of $M(CH_2NMe_2BH_3)_3$ Compounds

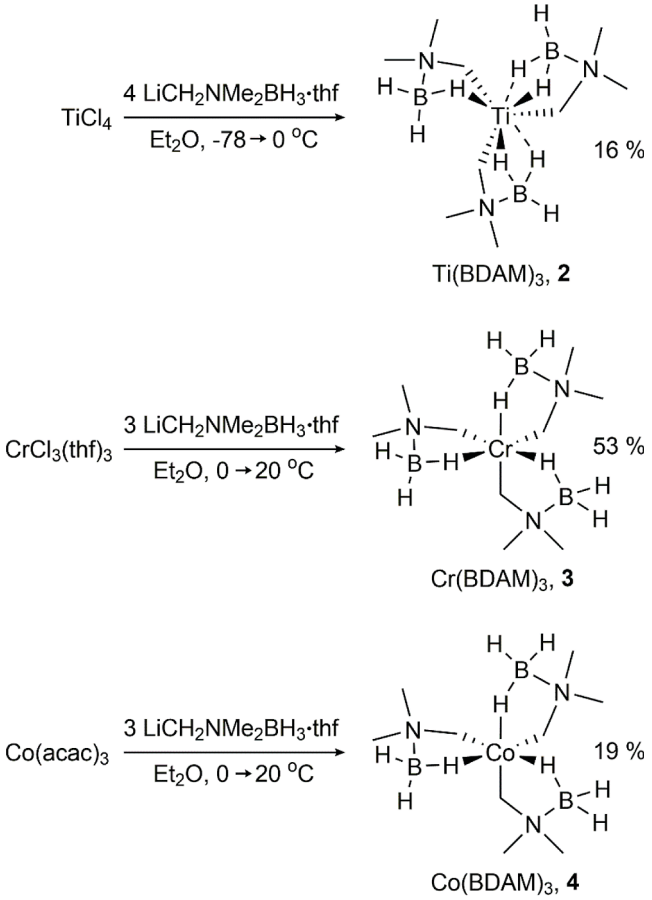

Treatment of $CrCl_3(thf)_3$ with three equiv of **1** at 0 °C in diethyl ether results in a red solution from which deep red needles of $Cr(BDAM)_3$ (**3**) can be obtained by crystallization. Solid samples of **3**, which can be sublimed at ∼60 °C under a vacuum, are stable under an atmosphere of argon for weeks. In solution, **3** is stable for hours under argon but decomposes immediately upon exposure to air.

Similarly, $Co(acac)_3$ reacts readily with three equiv of **1** at 0 °C in diethyl ether to produce a yellow-orange solution from which orange crystals can be obtained either by crystallization or by sublimation at ∼60 °C. The product, $Co(BDAM)_3$ (**4**), which can be isolated in yields of 10−25%, is stable under argon for hours in solution at room temperature and for months as a solid. In air, solutions and solid samples of **4** decompose over the course of hours. We can also synthesize **4** by adding lithium reagent **1** to cobalt(II) starting materials such as $CoBr_2$; only the cobalt(III) compound **4** (and no cobalt(II) products) is obtained even if these latter reactions are carried out in the presence of chelating Lewis bases such as 1,2-dimethoxyethane (dme) or *N*,*N*,*N*′,*N*′-tetramethylethylenediamine (tmed).

Compounds **2**−**4** are moderately soluble in pentane and readily soluble in diethyl ether, thf, benzene, and toluene.

Crystal Structures of the $M(BDAM)_3$ Compounds. Crystal data and refinement parameters for **2**−**4** are given in Table S1, and relevant bond distances and angles are summarized in Table 1. In all three crystal structures (Figure 1), hydrogen atoms attached to boron were located in the difference maps, and their positions were refined.

Table 1. Selected Distances and Angles for the $M(CH_2NMe_2BH_3)_3$ Compounds[a,h]

	2	3	4
M−H (Å)	2.07(2),[d] 2.52(2)[e]	1.96(1)	1.76(2)
M···B (Å)	2.618(2),[f] 2.692(2)[g]	2.747(1)	2.580(1)
M−C (Å)	2.191(2)	2.077(1)	1.942(1)
M−H−B (deg)	105(1),[f] 109(1)[g]	119(1)	121(1)
H−M−H (deg)	77.8(8)	86.8(6)	87.1(7)
C−M−C (deg)	95.43(8)	96.07(4)	93.60(5)
C−M−H_{cis}[b] (deg)		80.3(4)	85.8(5)
C−M−H_{cis}[c] (deg)		97.6(4)	95.9(5)
C−M−H_{trans} (deg)		166.1(4)	172.2(5)

[a]Some of the values given are averaged over chemically equivalent bonds. [b]Intraligand angle. [c]Interligand angle. [d]Hydrides on a vertex of the trigonal prism. [e]Semibridging hydrides. [f]$\kappa^{1.5}$-BH_3. [g]κ^1-BH_3. [h]Displacement of boron atoms from the plane formed by the metal, carbon, and nitrogen atoms of a BDAM ligand.

In titanium compound **2**, the BH_3 group of one of the three BDAM ligands binds to Ti in a κ^1 fashion, but the BH_3 groups in the other two BDAM groups bind in a fashion that is intermediate between κ^1 and κ^2: each BH_3 group forms one short and one longer "semibridging" Ti−H interaction (see Supporting Information for details). If we ignore the semibridging Ti−H interactions, the Ti center is six-coordinate, and its geometry is best described as a distorted trigonal prism. This nonoctahedral geometry is expected for a d^1 ion bound to ligands that are exclusively σ-bonding (if the

https://doi.org/10.1021/jacs.3c07336
J. Am. Chem. Soc. 2023, 145, 23585−23599

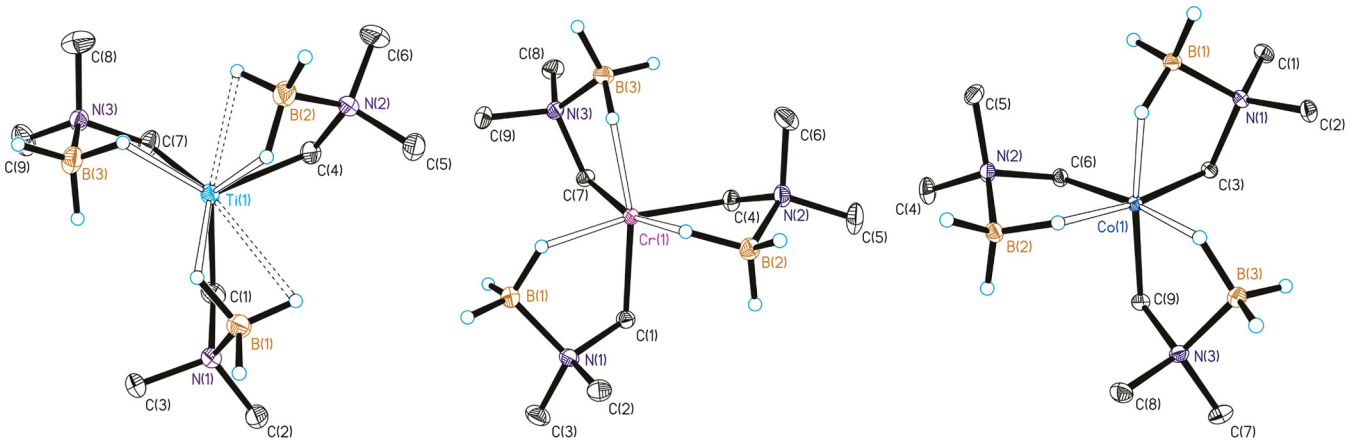

Figure 1. Molecular structures of $Ti(CH_2NMe_2BH_3)_3$ (**2**), $Cr(CH_2NMe_2BH_3)_3$ (**3**), and $Co(CH_2NMe_2BH_3)_3$ (**4**). Ellipsoids are drawn at the 35% probability level, except for the hydrogen atoms, which are represented as arbitrarily sized spheres. Dashed lines indicate semibridging interactions. Hydrogen atoms bound to carbon have been omitted for clarity.

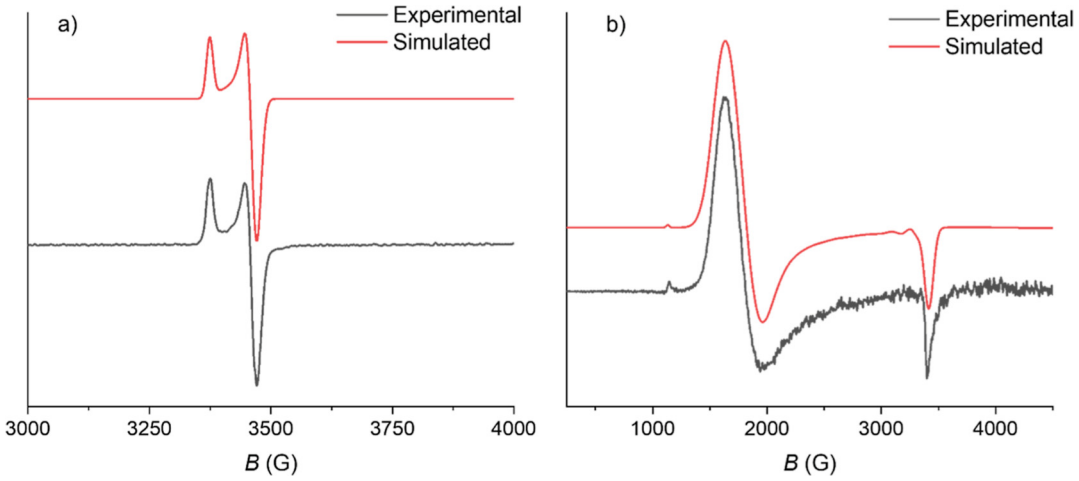

Figure 2. (a) X-band EPR spectrum of $Ti(CH_2NMe_2BH_3)_3$, **2**, as a frozen solution in toluene at 77 K (black) and its computed simulation (red). Experimental parameters: 9.417715 GHz microwave frequency, 2.000 mW microwave power, and 2.0 G modulation amplitude. Simulation parameters: g = {1.942, 1.942, 1.994}, line width = 3.7 G, anisotropic residual line width = {68, 68, 43} MHz. (b) X-band EPR spectrum of $Cr(CH_2NMe_2BH_3)_3$, **3**, as a frozen solution in toluene at 77 K (black) and its computed simulation (red). Experimental parameters: 9.418895 GHz microwave frequency, 7.962 mW microwave power, and 10.0 G modulation amplitude. The variation of the baseline noise as a function of B is an instrumental artifact. Simulation parameters: g = {1.978, 1.978, 1.980}, D = 22,175 MHz, E/D = 0.041, line width = 20 G, anisotropic residual line width = {1315, 1315, 250} MHz.

ligands had π-donor character, the coordination geometry would be octahedral).[33] If the two additional semibridging Ti−H interactions are included, the coordination geometry of compound **2** is a distorted eight-coordinate bicapped trigonal prism.[34] The ability of titanium(III) to form these additional interactions is not unexpected because there are eight empty valence orbitals in a d^1 ion. Similar semibridging M−H−B interactions have been noted in the aminoborane complex $(L)Ag(\kappa^{1,5}\text{-}BH_3NMe_3)$ (L = 2,6-bis-[1-(2,6-diisopropylphenylimino)ethyl]pyridine), in which one of the M−H−B interactions is ∼0.2 Å shorter than the other.[35]

The chromium(III) and cobalt(III) compounds **3** and **4** are isomorphous with one another: both compounds can be considered as having six-coordinate *fac*-octahedral geometries with idealized 3-fold symmetry (C_3 point group), in which three carbon atoms and three hydrogen atoms (or B−H units) form the six ligating groups. In these compounds, all three BH_3 groups clearly interact with the metal in a κ^1 fashion through one bridging hydrogen atom (Figure 1). The absence of semibridging interactions in these d^3 and low-spin d^6 compounds is a consequence of the availability of only six empty valence orbitals on the metal center vs eight for titanium(III).

The M−C and M···B distances in compounds **2**−**4** generally fall in the range of those reported for similar organometallic and borohydride compounds. For a detailed discussion of these structural comparisons, see Supporting Information.

IR Spectra of the M(BDAM)$_3$ Compounds. The IR spectra of the $M(BDAM)_3$ compounds display characteristic B−H stretching bands for metal-bound borohydride groups, which lie between ∼1800 and 2600 cm^{-1} (Figure S10). For titanium compound **2**, the absorptions in this region are not well resolved into distinct sets of bands due to bridging and terminal B−H stretches (as is usually the case), likely due to the presence of the semibridging B−H groups as discussed above. The calculated B−H stretching frequencies of **2** (UB3LYP/def2-TZVPP) fall into three distinct groups separated from one another by ∼100 cm^{-1} (Figure S19). In

https://doi.org/10.1021/jacs.3c07336
J. Am. Chem. Soc. 2023, 145, 23585−23599

order of increasing frequency, these bands are the symmetric and antisymmetric stretching modes of (1) bridging B−H bonds, (2) semibridging B−H bonds, and (3) terminal B−H bonds. This ordering is in agreement with the expectation that the B−H stretching frequency should increase as the Ti−H interaction becomes weaker. The spectra of the cobalt and chromium compounds **3** and **4** are similar to one another and differ from the spectrum of **2**: they display two distinct sets of bands in the B−H stretching region due to the stretching modes of bridging (lower frequency) and terminal (higher-frequency) B−H bonds.[36]

It has previously been suggested that a larger frequency difference between the bridging and terminal B−H stretches of a borohydride group indicates a stronger interaction with the metal center (i.e., greater weakening of the bridging B−H bonds and greater strengthening of the terminal B−H bonds).[37,38] The frequency difference of ∼400 cm^{-1} in compounds **2**−**4** is greater than the ∼100−250 cm^{-1} difference typically seen for borohydride complexes of lanthanide[36] and alkaline earth[39,40] metals but is similar to the ∼300−500 cm^{-1} difference typically seen for borohydride complexes of the transition metals.[41] This comparison suggests that the metal-borohydride interactions in these compounds are relatively strong. This conclusion is relevant to the interpretation of the UV−vis spectra, which is discussed below.

EPR Spectra of Ti(BDAM)$_3$ and Cr(BDAM)$_3$. The EPR spectra of the paramagnetic titanium and chromium compounds **2** and **3** were collected as frozen toluene solutions (Figure 2). The EPR spectrum of the S = 1/2 titanium compound **2** can be simulated with an axially restricted g tensor of $\{g_\perp = 1.942, g_\parallel = 1.994\}$, a Gaussian line width of 3.7 G, and an axially restricted anisotropic residual line width tensor of {68, 68, 43} MHz. Hyperfine coupling to ^{47}Ti (I = 5/2, 7.75% abundant) or ^{49}Ti (I = 7/2, 5.51% abundant) is not clearly present. The axial nature of the spectrum is consistent with the crystal structure of **2**, whose coordination geometry approximates to a trigonal prism; the values of $g_\perp$ = 1.942 and $g_\parallel$ = 1.994 are similar to those of other titanium(III) compounds with axial symmetry.[42−44]

For the S = 3/2 compound **3**, the relevant spin Hamiltonian is $H_s = \mu_B B{\cdot}g{\cdot}\hat{S} + D[S_z^2 - 1/3S(S+1) + \lambda(S_x^2 - S_y^2)]$, where μ_B is the Bohr magneton, B is the magnetic field vector, g is the electronic Landé g-tensor, $\hat{S}$ is the electronic spin operator (and S is the spin quantum number), D is a zero-field splitting parameter, and λ is a symmetry parameter that can vary from zero for axial symmetry to one-third for maximum possible rhombic symmetry. The EPR spectrum of **3**, which contains a broad signal at $g'_\perp \approx 4$ and a weaker signal at $g'_\parallel \approx 2$, resembles those of other S = 3/2 six-coordinate chromium(III) alkyls with large values of D and little rhombicity ($\lambda \approx 0$).[45] The small peak at $g' \approx 6$ can be attributed to the formally forbidden Δm_s = 3 transition, which becomes weakly allowed as λ deviates from zero.[45]

The experimental spectrum of **3** can be successfully simulated with an axially restricted g tensor of $\{g_\perp = 1.978, g_\parallel = 1.980\}$, a symmetry parameter λ of 0.041, a Gaussian line width of 2.0 G, and an axially restricted anisotropic residual line width tensor of {1315, 1315, 250} MHz. For this system, the EPR spectrum at field strengths up to 10,000 G is essentially insensitive to the exact magnitude of the zero-field splitting parameter D if $|D|$ is large; for **3**, we can determine a lower limit of $|D| > \sim 20{,}000$ MHz (i.e., 1.5 cm^{-1}). The nonzero symmetry factor of 0.041 and the weak intensity of the feature at $g' \approx 6$ both are consistent with a slight deviation from axial symmetry.

Variable Temperature NMR Spectra of M(BDAM)$_3$ Compounds (M = Cr, Co). Even though the chromium and cobalt compounds **3** and **4** have kinetically inert pseudo-octahedral d^3 and low-spin d^6 electron configurations, respectively, they both exhibit dynamic processes in solution, as shown by their NMR spectra. We will defer our discussion of chromium compound **3** to a later section because its paramagnetism complicates the analysis of its dynamic behavior.

For the diamagnetic cobalt compound **4**, we expect to see three ^{1}H NMR resonances for the BH_3 groups (one for the bridging H atom and two more for the diastereotopic terminal H atoms), but instead at room temperature (Figure 3), all

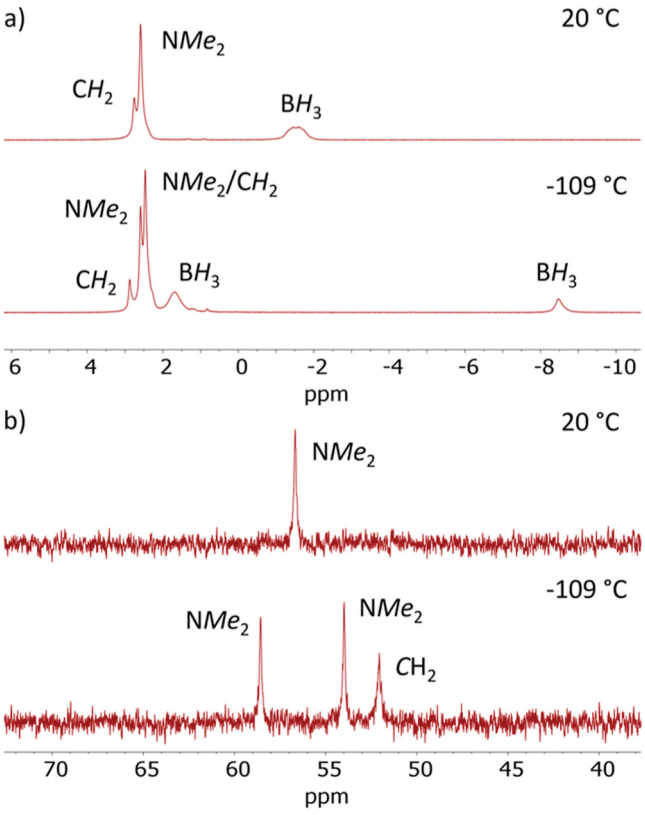

Figure 3. (a) ^{1}H NMR spectra of $Co(CH_2NMe_2BH_3)_3$, **4**, at 20 °C (top) and −109 °C (bottom) in $CDFCl_2$. (b) $^{13}C\{^1H\}$ NMR spectra of $Co(CH_2NMe_2BH_3)_3$, **4**, at 20 °C (top) and −109 °C (bottom) in $CDFCl_2$.

three hydrogen atoms give rise to a single BH_3 resonance (verified by integration). In the crystallographically determined *fac*-octahedral structure of **4**, the two hydrogen atoms of each CH_2 unit and the two methyl groups of each NMe_2 unit are diastereotopic, but the room-temperature ^{1}H NMR spectrum displays only one CH_2 and only one NMe_2 resonance (Figure 3). Similarly, the $^{13}C\{^1H\}$ NMR spectrum of **4** at room temperature displays only one NMe_2 resonance instead of two (Figure 3); there is also a broad resonance for the CH_2 carbons (to be discussed in more detail below).

The observations above suggest that the cobalt compound **4** undergoes two dynamic processes in solution: (1) BH_3 rotation that exchanges the terminal and bridging B−H hydrogen atoms, and (2) Δ/Λ racemization that exchanges

https://doi.org/10.1021/jacs.3c07336
J. Am. Chem. Soc. 2023, 145, 23585−23599

the diastereotopic NMe_2 methyl groups and CH_2 hydrogen atoms.

These dynamic processes can be slowed (and decoalescence observed) at lower temperatures. At −109 °C, the ^1H NMR spectrum of **4** contains two broad BH_3 resonances near δ 1.6 and −8.5 (with intensities in a 2:1 ratio), corresponding to the terminal and bridging B−H hydrogen atoms, respectively, in addition to two equal-intensity NMe_2 resonances and two CH_2 resonances (one of which lies under the NMe_2 peaks). At −109 °C, the $^{13}C\{^1H\}$ NMR spectrum of **4** displays resonances at δ 58.5 and 53.9 for the two diastereotopic NMe_2 carbon atoms and one resonance near δ 52 for the CH_2 carbon atoms bound to cobalt (Figure 3). Both the ^1H and $^{13}C\{^1H\}$ NMR spectra at low temperature are consistent with the solid-state structure of **4**, although the diastereotopic terminal B−H hydrogen atoms evidently have the same ^1H NMR chemical shift by accident. The ^1H NMR chemical shift of δ −1.6 for the BH_3 group at room temperature is nearly identical with that of δ −1.7 for the weighted average of the bridging and terminal B−H chemical shifts in the slow exchange regime.

Computer simulations (WinDNMR[46]) of the variable-temperature ^1H and $^{13}C\{^1H\}$ NMR line shapes of **4** afford rates for the two exchange processes (Figures 4 and 5). An

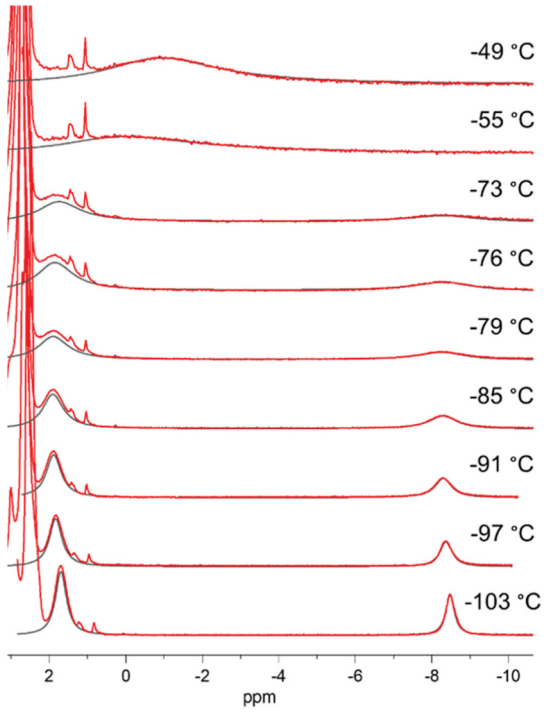

Figure 4. Variable-temperature ^1H NMR spectra of BH_3 resonances of $Co(CH_2NMe_2BH_3)_3$, **4**, (red), and overlaid simulated spectra (black) at each measured temperature.

Eyring plot of the BH_3 rotation rate at nine different temperatures between −103 and −49 °C gives the activation parameters $\Delta H^‡$ = 7.4 ± 0.4 kcal mol^{-1} and $\Delta S^‡$ = −6.8 ± 2.3 cal·mol^{-1}·K^{-1} (Figure S12 and Table 2). These parameters correspond to a free energy of activation of $\Delta G^‡$ = 9.4 ± 0.1 kcal mol^{-1} at 298 K.[47]

The Δ/Λ racemization rate of **4** was determined through analysis of the line shapes of ^1H NMR resonances for both the NMe_2 and CH_2 groups, as well as of the $^{13}C\{^1H\}$ NMR resonances of the NMe_2 groups, at selected temperatures between −109 and −58 °C (Figure 5). Fitting the measured rates to the Eyring equation gives $\Delta H^‡$ = 6.5 ± 0.4 kcal mol^{-1}, $\Delta S^‡$ = −11.8 ± 2.4 cal mol^{-1} K^{-1}, and $\Delta G^‡_{298\ K}$ = 10.1 ± 0.1 kcal mol^{-1} from the ^1H NMR data, and $\Delta H^‡$ = 6.4 ± 0.5 kcal mol^{-1}, $\Delta S^‡$ = −11.9 ± 2.7 cal mol^{-1} K^{-1}, and $\Delta G^‡_{298}$ = 10.0 ± 0.1 kcal mol^{-1} from the $^{13}C\{^1H\}$ NMR data (Figure S13 and Table 2). These values agree well with each another.

We attribute the narrowing of the $^{13}C\{^1H\}$ NMR resonance near δ 52.7 for the CH_2 group of compound **4** at lower temperatures (Figure 5) to a thermal decoupling of ^{59}Co and ^{13}C nuclei due to the temperature-dependence of the quadrupolar relaxation rate[48−51] of cobalt atoms (^{59}Co has I = 7/2 and 100% natural abundance, see Supporting Information for further discussion).

The chromium(III) compound **3** appears to undergo similar dynamic processes in solution, but its paramagnetism complicates the exact determination of rates from variable-temperature ^1H NMR line shapes. However, the barrier for Δ/Λ racemization can be estimated (see Supporting Information), giving $\Delta G^‡ \approx$ 6 kcal mol^{-1} at −109°; this activation energy for **3** is similar to the $\Delta G^‡$ value of 8.4 kcal mol^{-1} seen for the cobalt compound **4**.

DFT Studies of the Mechanism of the BH_3 Rotation Process in $Co(BDAM)_3$. Two mechanisms for BH_3 rotation are plausible: (1) a dissociative mechanism in which the κ^1-BH_3 groups dissociate, rotate, and reassociate, and (2) a nondissociative mechanism in which the κ^1-BH_3 groups rotate in place via a κ^2 transition state, in which the cobalt center is seven-coordinate. The small negative entropy of the activation parameter is more consistent with the nondissociative mechanism. This conclusion is supported by DFT calculations (see Supporting Information for details), which show that the κ^2 transition state (Figure S20) corresponding to the nondissociative rotation of one BH_3 group has a relative energy of 7.6 kcal mol^{-1} at 298 K. The nondissociative nature of this process is shown by the Co···B distances in TS_1 of 2.61 (κ^2), 2.62 (κ^1), and 2.66 (κ^1) Å, which are all very similar (Table S4). The BH_3 rotation barrier in **4** of 7.6 kcal mol^{-1} is in good agreement with those of 7.6 and 7.0 kcal mol^{-1} in $Cr(CO)_5(BH_3NMe_3)$ and $CpMn(CO)_2(BH_3PMe_3)$, respectively, both of which proceed (according to DFT studies) through seven-coordinate transition states.[52]

DFT Studies of the Mechanism of the Δ/Λ Racemization Process in $Co(BDAM)_3$. Octahedral cobalt(III) compounds almost always have large activation free energies for the Δ/Λ racemization process; in fact, most are stereochemically rigid on the NMR time scale (and even on the chemical time scale).[53−56] To our knowledge, the only exceptions to this generalization are cobalt tris(tropolonate) and tris(dithiocarbamate) complexes, in which the ligands potentially are electronically non-innocent; these complexes have activation free energies $\Delta G^‡$ of between 14 and 15 kcal mol^{-1} at either 5 or 25 °C.[53,57,58] As shown from the variable temperature NMR studies above, BDAM complex **4** has by far the smallest Δ/Λ racemization barrier ($\Delta G^‡$ = 10.1 kcal mol^{-1} at 25 °C) seen for any octahedral cobalt(III) complex.

For cobalt(III) tris-chelate coordination compounds, two commonly invoked Δ/Λ racemization mechanisms are dissociative processes (in which one metal−ligand bond is broken to afford a five-coordinate intermediate) and non-dissociative twist processes (there are two variants of twist mechanisms: the Bailar twist and the Ray-Dutt twist). Small

https://doi.org/10.1021/jacs.3c07336
J. Am. Chem. Soc. 2023, 145, 23585−23599

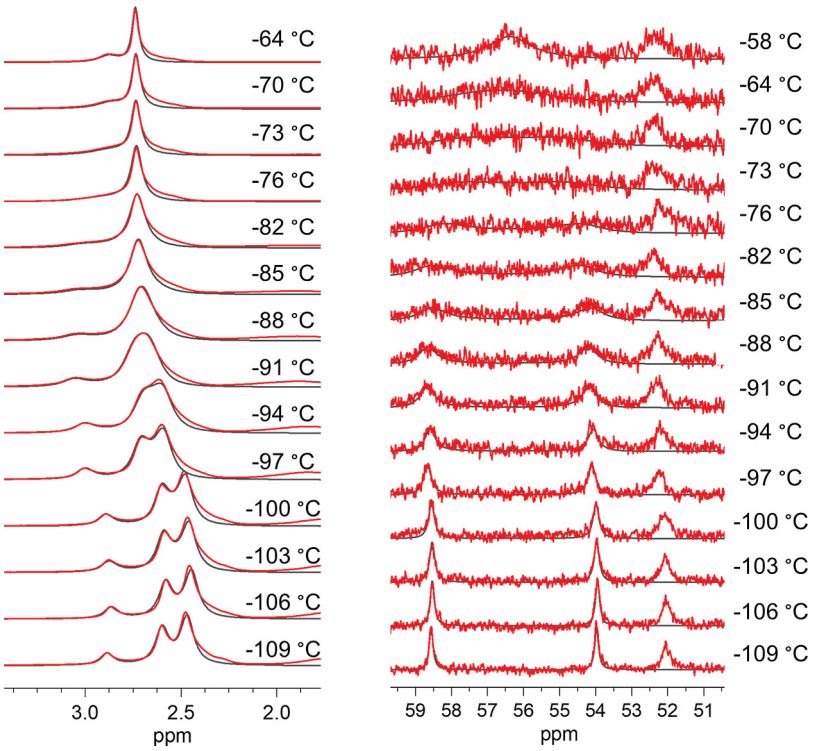

Figure 5. Variable-temperature ^{1}H (left) and ^{13}C{^{1}H} (right) NMR spectra of methyl and methylene resonances of Co($CH_2NMe_2BH_3$)$_3$, **4**, (red), and overlaid simulated spectra (black) at each measured temperature. The nonexchanging peak at δ 52 in the ^{13}C{^{1}H} NMR spectrum is the Co-CH_2 resonance.

Table 2. Activation Parameters Measured for Dynamic Processes in Co($CH_2NMe_2BH_3$)$_3$, 4

	$\Delta G^{\ddagger}_{298K}$ (kcal mol^{-1})	$\Delta H^{\ddagger}$ (kcal mol^{-1})	$\Delta S^{\ddagger}$ (cal·mol^{-1}·K^{-1})
BH_3 rot.	9.4 ± 0.1	7.4 ± 0.4	−6.8 ± 2.3
Δ/Λ^a	10.1 ± 0.1	6.5 ± 0.4	−11.8 ± 2.4
Δ/Λ^b	10.0 ± 0.1	6.4 ± 0.5	−11.9 ± 2.7

[a]Measured from variable-temperature ^{1}H NMR data. [b]Measured from variable-temperature ^{13}C{^{1}H} NMR data.

positive entropies of activation are indicative of dissociative mechanisms, whereas small negative entropies of activation are indicative of nondissociative twist mechanisms.[55,57] For **4**, the negative entropy of activation (−11.8 ± 2.4 cal mol^{-1} K^{-1}) for the Δ/Λ racemization is more consistent with a non-dissociative mechanism.

For compounds **2**, **3**, and **4**, the crystallograpically determined face twist angles are 3.8, 45.1, and 51.3°, respectively.[59] The geometry of the titanium complex is clearly close to the ideal twist angle of 0° for a trigonal prism, whereas the geometries of the chromium and cobalt complexes are octahedral but twisted by 10−15° away from the ideal angle of 60°. For the chromium and cobalt compounds **3** and **4**, the deviations of the twist angle away from their ideal indicate that a twist mechanism−and in particular a Bailar twist[60] − could be responsible for the racemization of the M(BDAM)$_3$ compounds.

We have used DFT calculations to analyze the mechanism by which **4** racemizes (see the Supporting Information for details). In the following discussion, we use the symbols Δ and Λ to indicate the overall handedness of the molecule and the symbols δ and λ to indicate the ring conformation of an individual ligand (the BDAM ligands are nonplanar and can be puckered in two ways).

Although most Δ/Λ racemizations of low-spin cobalt(III) complexes are nondissociative and take place by a Bailar twist, the DFT studies suggest that the lowest energy racemization pathway of **4** is more complicated than this (Figure 6). Beginning from the Δ enantiomer, the first step in this pathway (Figure 6, TS_2) involves the dissociation of one BH_3 group (i.e., from κ^1 to κ^0; the calculated Co···B distance increases from 2.62 to 3.14 Å), while at the same time, another BH_3 group changes from κ^1 to κ^2 (its Co···B distance decreases from 2.62 to 2.40 Å). The third ligand remains κ^1-BH_3 but inverts to a λ conformation owing to a twisting motion that resembles a Bailar twist. The calculated value of $\Delta G^{\ddagger}$ = 11.8 kcal mol^{-1} for TS_2 is in agreement with the measured value of the racemization barrier of $\Delta G^{\ddagger}$ = 10.1 kcal mol^{-1}. The low barrier for this dissociative process reflects the fact that the breaking of one M−H interaction (i.e., one BH_3 group changes from κ^1 to κ^0) is compensated for by the simultaneous formation of another M−H interaction (i.e., another BH_3 group changes from κ^1 to κ^2). Similar κ^1 to κ^2 hemilability of borohydride ligands has also been observed in a compound containing a chelating phosphinoboranate ligand.[13]

This first step affords a six-coordinate pseudo-octahedral intermediate in which the cobalt atom is bound to the carbon atoms of all three ligands, to one κ^1-BH_3 group, and to one κ^2-BH_3 group; the third BDAM ligand is bound in a unidentate fashion (i.e., with a κ^0-BH_3 group). After passing through TS_2, the complex can arrive at either of two intermediates: one in which the κ^0 BH_3 group remains near the bound BH_3 groups (INT_1, ΔG = 6.1 kcal mol^{-1}) or another in which rotation about the C−N bond brings one of the nitrogen-bound methyl groups near the bound BH_3 groups (INT_2, ΔG = 7.6 kcal

https://doi.org/10.1021/jacs.3c07336
J. Am. Chem. Soc. 2023, 145, 23585−23599

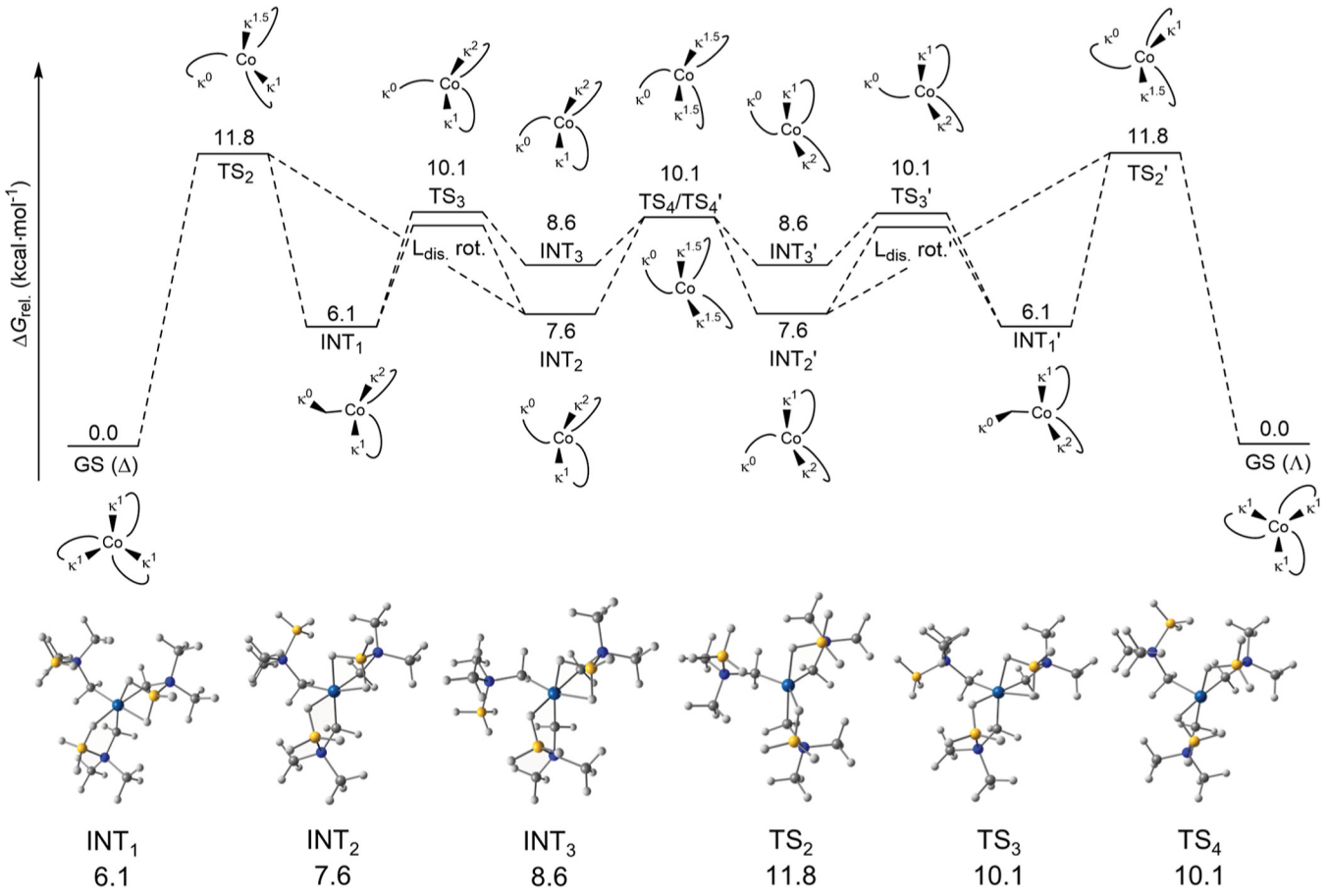

Figure 6. (top) Gibbs free energy diagram for the dissociative racemization pathway of $Co(CH_2NMe_2BH_3)_3$, **4**. κ^n indicates a BH_3 group bound to Co through *n* bridging hydrides. Primes indicate mirror images. (bottom) Molecular structures and calculated relative free energies (kcal mol^{-1}) of intermediates and transition states found for the dissociative racemization pathway of $Co(CH_2NMe_2BH_3)_3$, **4**. All calculations were performed at the B3LYP/def2-TZVPP level of theory at 298.15 K, and energies were obtained employing a solvent field correction (chloroform, ε = 5.34). All free energies are reported relative to the ground-state DFT-optimized structure of **4**.

mol^{-1}). From INT_1 or INT_2, structural rearrangements must occur, ultimately reaching INT_1' or INT_2' of the opposite handedness, in order for reassociation of the κ^0 BH_3 group (via TS_2') to result in racemization. These rearrangements consist of conformational changes of the dissociated ligand combined with an exchange process in which the κ^1-BH_3 group becomes κ^2 while the κ^2-BH_3 group becomes κ^1. Both processes are calculated to have low activation barriers: the ligand can change its conformation from INT_1 to INT_3 via a transition state (TS_3) with $\Delta G^{\ddagger}$ = 4.0 kcal mol^{-1}, and the $\kappa^1 \leftrightarrow \kappa^2$ exchange from INT_3 to INT_2' proceeds through a transition state (TS_4) with $\Delta G^{\ddagger}$ = 2.5 kcal mol^{-1} (Figure 6).

The Δ/Λ racemization of **4** can also take place by a pure twist mechanism, although the computed barrier for this process is somewhat higher (Figure 7), and even this pathway involves a step having dissociative character. Initial attempts to locate a nondissociative transition state with C_{3v} symmetry (i.e., a trigonal prism with three planar κ^1-BH_3 ligands corresponding to a classical Bailar twist) invariably diverged into structures of lower symmetry with puckered conformations of the ligands. Calculations show that conversion of the Δ-*δδδ* ground state to its Δ-*λλλ* enantiomer does not occur in one concerted movement, but instead, the inversions of the ligand conformations and the Bailar twist occur in separate steps. Starting from the Δ-*δδδ* ground state, one ligand inverts to give a Δ-*λδδ* intermediate with a computed barrier of $\Delta G^{\ddagger}$ = 2.1 kcal mol^{-1} (TS_5 in Figure 7). Subsequent ligand inversions (which should have similarly low barriers) give the Δ-*λλλ* intermediate (INT_4 in Figure 7), which lies only 3.7 kcal mol^{-1} above the ground state. We found that this Δ-*λλλ* intermediate can convert into the Λ-*λλλ* ground state structure (which is the enantiomer of the Δ-*δδδ* starting point) via a C_3 symmetric transition state (TS_6 in Figure 7). This transition state involves a Bailar-twist motion of the inner coordination sphere, in which the puckering conformations of the three individual ligands are retained. In addition to the twisting motion, all three Co−H bonds lengthen from 1.75 Å in the ground state (and 1.73 Å in INT_4) to 2.04 Å in TS_6 (Table S4). Thus, the twisting motion from the Δ-*λλλ* intermediate to the final Λ-*λλλ* structure has considerable dissociative character.

This Δ-*δδδ* ⇌ Δ-*λδδ* ⇌ Δ-*λλδ* ⇌ Δ-*λλλ* ⇌ Λ-*λλλ* pathway, paired with its mirror image Λ-*λλλ* ⇌ Λ-*δλλ* ⇌ Λ-*δδλ* ⇌ Λ-*δδδ* ⇌ Δ-*δδδ*, satisfies the principle of microscopic reversibility. The calculated overall barrier for this nondissociative process, $\Delta G^{\ddagger}$ = 14.5 kcal mol^{-1}, is only slightly higher than the 11.8 kcal mol^{-1} calculated barrier for the dissociative mechanism that involves breaking the Co−H bond of a single BDAM ligand; the similarity in the barriers (to one another and to the measured value of 10.1 ± 0.1 kcal mol^{-1}) suggests that both mechanisms may occur in solution.[34]

https://doi.org/10.1021/jacs.3c07336
J. Am. Chem. Soc. 2023, 145, 23585−23599

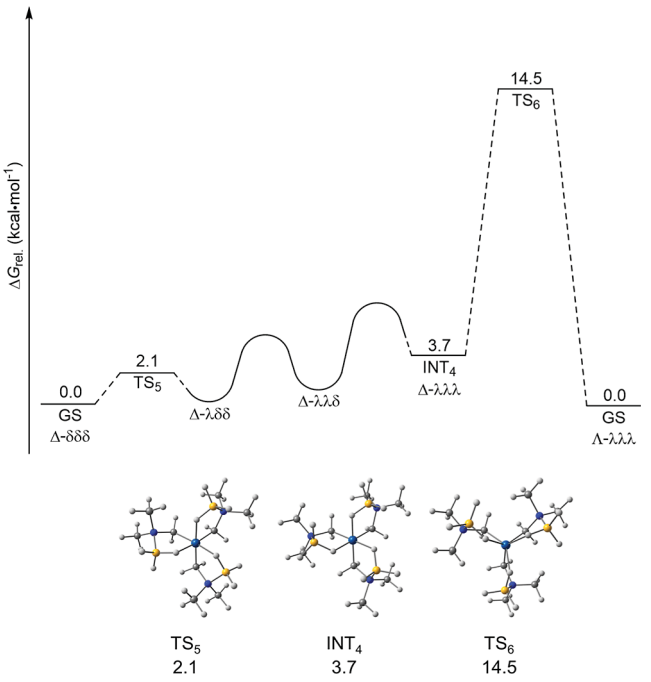

Figure 7. Top: Gibbs free energy diagram for the pseudotwist racemization pathway of $Co(CH_2NMe_2BH_3)_3$, **4**. Δ/Λ indicates the handedness of the molecule; δ/λ indicates the conformation of individual ligands. Bottom: molecular structures and calculated relative free energies (kcal mol^{-1}) of intermediates and transition states found for the pseudotwist racemization pathway of $Co(CH_2NMe_2BH_3)_3$, **4**. All calculations were performed at the B3LYP/def2-TZVPP level of theory at 298.15 K, and energies were obtained employing a solvent field correction (chloroform, ε = 5.34). All free energies are reported relative to the ground-state DFT-optimized structure of **4**.

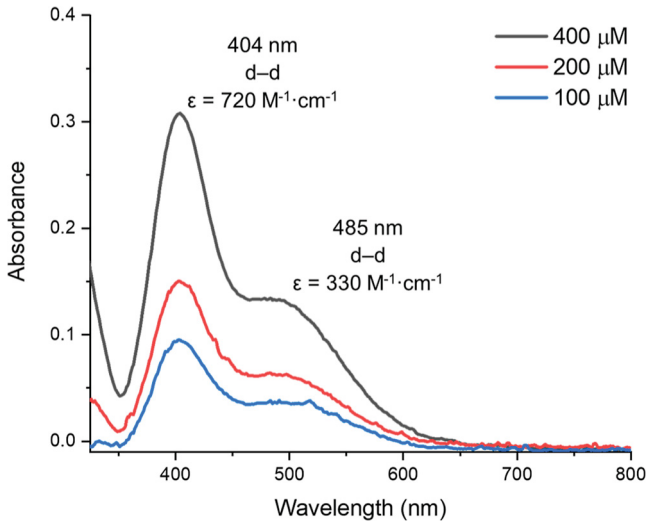

Figure 8. UV−vis absorption spectrum of $Cr(CH_2NMe_2BH_3)_3$, **3**, in diethyl ether.

Finally, we point out that the negative entropy of activation measured experimentally for this Δ/Λ racemization process is probably consistent with both of the mechanisms discussed above. Both mechanisms involve steps that combine associative and dissociative character and that simultaneously add and subtract degrees of freedom.

Ligand Field Properties of $Cr(BDAM)_3$ and $Co(BDAM)_3$. The pseudo-octahedral geometries of the chromium(III) and cobalt(III) boranatodimethylaminomethyl compounds provide an opportunity to measure the ligand field strength of the BDAM ligand by analysis of their UV−visible absorption spectra. The UV−vis spectrum of the chromium compound **3** contains two bands at 404 and 485 nm (Figure 8), with molar absorption coefficients of 720 and 330 M^{-1} cm^{-1} that are similar to the values of 100 M^{-1} cm^{-1} typically seen for spin-allowed, Laporte-forbidden d−d bands in chromium(III) complexes.[61−63] The absence of detectable splittings in the d−d bands indicates that the crystal field symmetry of **3** does not deviate significantly from octahedral, so that the 3d orbitals can still be grouped into near-degenerate sets of effective t_{2g} and e_g symmetry. Accordingly, we treat **3** (and the isostructural cobalt analogue **4**) as belonging to the O_h point group in the following section.

For octahedral d^3 ions, there are three spin-allowed electronic transitions: two of these, $^4A_{2g} \rightarrow {}^4T_{2g}$ and $^4A_{2g} \rightarrow {}^4T_{1g}(F)$, are typically in the visible region, whereas the third transition, $^4A_{2g} \rightarrow {}^4T_{1g}(P)$, is typically in the UV. According to ligand field theory,[64] the lowest energy transition $^4A_{2g} \rightarrow {}^4T_{2g}$ has an energy given by Δ_o, where Δ_o is the octahedral splitting (sometimes called 10Dq). From the location of the lowest energy band for **3** at 485 nm, we can directly determine that Δ_o = 20,600 cm^{-1}.

The d-orbital field splitting Δ_o = 20,600 cm^{-1} for **3** is compared with the Δ_o values for other chromium(III) complexes in Table 3. In interpreting the values, we assume that the d-orbital splitting of an unsymmetrical tris(chelate) complex $M(XY)_3$ is the average of the splittings of the related $M(XX)_3$ and $M(YY)_3$ complexes having symmetrical chelating ligands[65] and that the total splitting is the sum of the splittings caused by each of the six coordinating groups. The results suggest that the splitting caused by the BDAM ligand (i.e., the combined splitting caused by the two ends of the chelate) is similar to that of two alkyl groups. This result in turn shows that the ligand field splittings induced by borohydride ligands are similar to those caused by alkyl groups, which are considered to lie near cyanide, i.e., relatively high in the spectrochemical series.[66]

This conclusion is unexpected because three-center-two-electron M−H−B interactions are frequently considered to be weak.[13,17,21,26,27] The field strength of a ligand is larger if it is a strong π-acceptor (so it stabilizes the t_{2g} orbitals of an octahedral complex) or a strong σ-donor (so it destabilizes the e_g* orbitals of an octahedral complex) or both. Borohydride ligands are certainly not π-acceptors and are not generally considered to be strong σ-donors, so the high ligand field strength of the BDAM ligand is somewhat surprising.

It is of interest to determine whether BDAM also serves as a strong field ligand for cobalt(III). The absorption spectrum of **4** (Figure 9) contains two bands at 352 and 442 nm, with molar absorptivity coefficients (ε = 430 M^{-1} cm^{-1} at 352 nm, ε = 270 M^{-1} cm^{-1} at 442 nm) that are comparable to those seen for other cobalt(III) complexes.[64,67]

We assign the two bands to the spin-allowed $^1A_{1g} \rightarrow {}^1T_{2g}$ and $^1A_{1g} \rightarrow {}^1T_{1g}$ transitions typically seen for low-spin d^6 transition metal complexes,[64] and these assignments were confirmed by a simulation of the spectrum with time-dependent density functional theory (TD-DFT). The calculated natural transition orbitals (NTOs) for the relevant states confirm that the features centered at 352 and 442 nm are, in

https://doi.org/10.1021/jacs.3c07336
J. Am. Chem. Soc. 2023, 145, 23585−23599

Table 3. Ligand Field Parameters for Various Octahedral Low-Spin Chromium(III) and Cobalt(III)[a] Complexes

cmpd	Δ_o (cm^{-1})	ref	cmpd	Δ_o (cm^{-1})	B (cm^{-1})[b]	C (cm^{-1})	ref
CrI_3	11,700	68	$Co(acac)_3$	19,210	480	3590	67
$[Cr(H_2O)_6]^{3+}$	17,400	69	$[Co(NH_3)_6]^{3+}$	23,430	580	3550	67
$[Cr(CCSiMe_3)_6]^{3-}$	20,200	70	$[Co(en)_3]^{3+}$	23,950	500	3640	67
$Cr(BDAM)_3$	20,400	this work	$[Co(bpy)_3]^{3+}$	24,480	560	3900	67
$[Cr(CH_3)_6]^{3-}$	20,800	63	$Co(BDAM)_3$	24,760	410	2960	this work
$[Cr(NH_3)_6]^{3+}$	21,600	69	$[Co(CN)_6]^{3-}$	34,160	510	3080	67
$[Cr(CN)_6]^{3-}$	26,600	62					

[a]Ligand field parameters for all cobalt(III) complexes were determined through observation of at least one spin-forbidden transition and calculated through full matrix diagonalization. [b]B(free Co^{III} ion) = 1100 cm^{-1}.

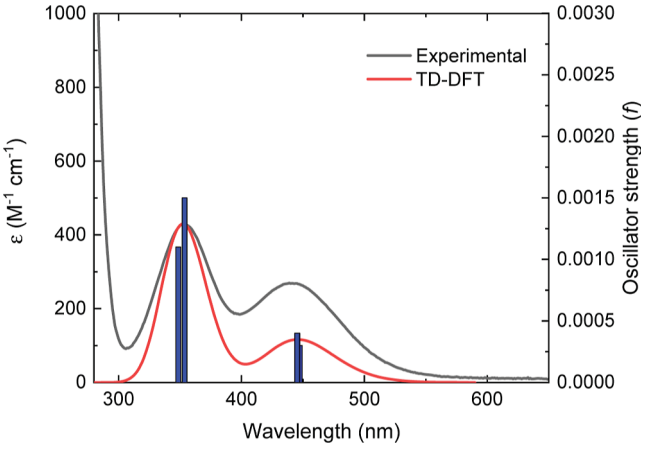

Figure 9. Overlay of experimental spectrum of $Co(CH_2NMe_2BH_3)_3$, **4**, (black) with simulated spectrum (red, Gaussian peak shapes with fwhm = 0.37 eV) and relevant oscillator strengths (blue) from TD-DFT calculations at the B3LYP/def2-TZVPP level.

fact, due to spin-allowed d−d transitions (see Supporting Information).

For low-spin d^6 complexes, the spin-allowed $^1A_{1g} \rightarrow {}^1T_{2g}$ and $^1A_{1g} \rightarrow {}^1T_{1g}$ transitions have energies that depend nonlinearly not only on Δ_o but also on two electron−electron repulsion terms B and C (often called Racah parameters).[67,72] If only the $^1A_{1g} \rightarrow {}^1T_{2g}$ and $^1A_{1g} \rightarrow {}^1T_{1g}$ transitions are experimentally observed, it is not possible to determine values for any of these three parameters unless an assumption is made; recent work has shown that a common assumption, that $C/B = 4$, is not generally applicable.[67] In order to calculate the parameters Δ_o, B, and C, a third transition must be observed; for an octahedral d^6 ion, the spin-forbidden $^1A_{1g} \rightarrow {}^3T_{2g}$ or $^1A_{1g} \rightarrow {}^3T_{1g}$ transitions are known to occur at lower energies than the two spin-allowed transitions mentioned above.

Although both spin-forbidden transitions for **4** were unobservable in a conventional 1 cm long cell, we were able to observe them by employing a significantly more concentrated solution and a cell with a 10 cm path length (Figure S11). We assign the absorption at 615 nm (ε = 180 $M^{-1}\cdot cm^{-1}$) to the spin-forbidden $^1A_{1g} \rightarrow {}^3T_{2g}$ transition; the absorption due to the $^1A_{1g} \rightarrow {}^3T_{1g}$ transition can be discerned, but the wavelength of its absorption maximum is uncertain. The first transition energy, however, combined with those of the two spin-allowed bands, is sufficient to enable us to determine the ligand field parameters Δ_o = 24,760 cm^{-1}, B = 410 cm^{-1}, and C = 2960 cm^{-1} by full-matrix diagonalization of the determinant representing the multielectronic term states of the d^6 configuration using an operator appropriate for O_h.[73] This diagonalization is conveniently performed with Bendix's LIGFIELD program.[74]

These parameters are compared with those of other cobalt(III) complexes (also determined through the observation of at least one spin-forbidden transition and calculated through full matrix diagonalization) in Table 3. The higher value of Δ_o for **4** than for $[Co(NH_3)_6]^{3+}$, $[Co(en)_3]^{3+}$, and $[Co(bpy)_3]^{3+}$ suggests that the average ligand field strength of alkyl and borohydride groups in cobalt(III) complexes is larger than that of amine ligands. This conclusion is again unexpected due to the frequent assumption that M−H−B interactions are considered to be weak.

The Racah parameters B and C are measures of the repulsion between pairs of electrons in doubly occupied metal d-orbitals: B for a metal complex (and the nephelauxetic parameter $\beta = B_{complex}/B_{free\ ion}$) decrease as electron−electron repulsion decreases.[65,67] Similar decreases in C are expected as electron−electron repulsion in occupied metal d-orbitals decreases, but there are comparatively few data reported for this parameter. Decreases in electron−electron repulsion are frequently attributed to π-acceptor interactions of the ligand with the metal or to delocalization of metal d-electrons onto polarizable ligands, both of which indicate that there is a large degree of covalency in the M−L interactions.[70,71]

The 410 and 2960 cm^{-1} values of B and C, respectively, for **4** are compared with those of other cobalt(III) complexes in Table 3 (the free ion value $B_{Co(III)}$ = 1100 cm^{-1}). The comparison suggests that the BDAM ligand can decrease electron−electron repulsions much more efficiently than cyanide, a π-acceptor. However, both the CH_2 and BH_3 ends of the BDAM ligand are σ-bonding only. Although the borohydride anion has been referred to as a "soft" and polarizable ligand,[75−77] aqueous BH_4^- has a polarizability slightly less than that of bromide,[78] which is not a particularly polarizable ion. The great ability of the BDAM ligand to decrease electron−electron repulsions must therefore be due to factors other than polarizability.

The results above suggest that the borohydride ligand lies relatively high on the spectrochemical series and is unusually effective in decreasing electron−electron repulsions. We will argue below, on the basis of electronic structure calculations, that the three-center-two-electron M−H−B interactions of borohydride ligands are partly responsible for their unexpected electronic properties.

ETS-NOCV Study of the M−H−B Interactions. To provide additional insights into the ligand-field properties of the BDAM ligand, extended-transition-state natural orbitals for chemical valence (ETS-NOCV) analyses were performed on $Co(BDAM)_3$, **4**. ETS-NOCV calculations have been extensively applied to elucidate metal−ligand bonding; of relevance

https://doi.org/10.1021/jacs.3c07336
J. Am. Chem. Soc. 2023, 145, 23585−23599

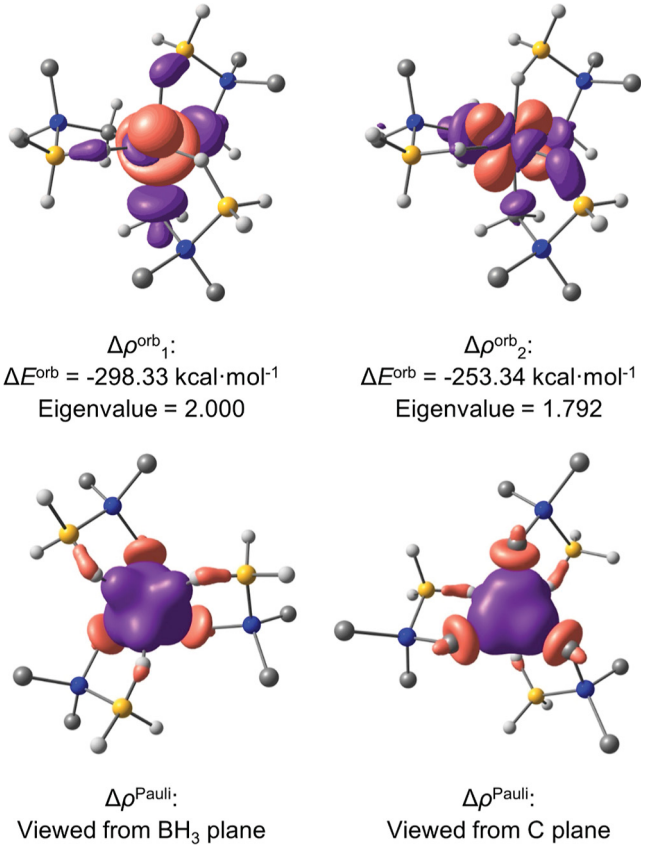

Figure 10. Top: major two NOCV deformation densities ($\Delta\rho^{orb}_i$, contour isovalue = 0.005) of $Co(CH_2NMe_2BH_3)_3$, **4**, and their associated energetic contributions (ΔE^{orb}), and electron transfer eigenvalues. Bottom: total electron density deformation as a result of Pauli repulsion ($\Delta\rho^{Pauli}$, contour isovalue = 0.001) for $Co(CH_2NMe_2BH_3)_3$, **4**. The image on the left is viewed from the BH_3 plane, and the image on the right is viewed from the *C* plane. The colors of the deformation densities indicate electron flow from purple to orange. Hydrogens of methyl groups have been omitted for clarity.

here is the use of this method to investigate agostic C−H−M[79−82] and covalent B−H−M interactions.[81,83−85]

The ETS-NOCV analysis was carried out with a fragmentation scheme consisting of Co^{3+} and $(BDAM)_3^{3-}$ fragments (Tables S8 and S9). The ΔE^{orb} terms for the first nine NOCV pairs sum to 95% of the total interaction energy between the fragments. Pairs 1 and 2 (Figure 10), which are responsible for 68% of the total interaction energy, involve the σ-donation of electron density from both the CH_2 and BH_3 termini of the BDAM ligands. The remaining pairs (excluding pair 5) correspond either to weak C → Co or BH_3 → Co σ-donations or to σ-back-donation from cobalt to the ligands. The acceptor orbitals (φ_i) in the latter correspond to either a lone pair on a CH_2 group or a B−H bonding orbital, and therefore, these Co → L NOCVs represent the degree of covalency in the metal−ligand bonds of **4** and are not indicative of weak Co → σ^*_{B-H} interactions. Pair 5 is a mixture of metal-to-ligand donation and reorganization of metal electron density, not clearly either L → Co or Co → L.

The eigenvalue associated with each NOCV pair represents the amount of electron transfer in the direction indicated by the corresponding isosurface. The total eigenvalues for the L → Co and Co → L interactions in **4** are 4.5 and 1.9, respectively, giving a net transfer of 2.6 electrons from the $(BDAM)_3^{3-}$ fragment to the Co^{3+} fragment (Table S10).

Because the UV−vis spectra discussed above suggested that the ligand field strength of a borohydride group is similar to that of ammonia (Table 3), we carried out an ETS-NOCV analysis of a model compound $Co(CH_3)_3(NH_3)_3$ that enables direct comparisons to be made between Co−H−B and Co−N interactions. The main NOCV pairs of $Co(CH_3)_3(NH_3)_3$ are very similar to those calculated for **4**: in both compounds, the two main NOCV pairs are L → Co σ-donating, and the minor NOCV pairs include one C → Co pair, one N or BH_3 → Co pair, two Co → C pairs, two N or BH_3 → Co pairs, and one unassignable pair (Tables S11 and S12). One notable difference is that the NOCV pairs corresponding to Co → BH_3 transfer in **4** involve a combination of both Co → H and B → H transfer, consistent with the presence of three-center-two-electron interactions.

The net ligand-to-metal electron transfer eigenvalues are 2.6 and 2.4 for **4** and $Co(CH_3)_3(NH_3)_3$, respectively (Tables S14 and S15); this result suggests that the BDAM ligand is a better donor than the combination of a methyl group and an ammonia ligand. More specifically, the larger eigenvalue of NOCV pair 7 for **4** (0.3, BH_3 → Co) vs that of pair 9 for $Co(CH_3)_3(NH_3)_3$ (0.2, N → Co) suggests that a BH_3 group in BDAM is a better donor than ammonia. We propose that the strong donor ability of the BH_3 group contributes significantly to the high ligand field strength of the BDAM ligand.

The similarity of the amount of L → Co and Co → L electron transfer in **4** and $Co(CH_3)_3(NH_3)_3$ indicates that the unusually small electron−electron repulsions (as indicated by the small Racah parameters *B* and *C*) measured for **4** are not due to an abnormally high degree of covalency in the metal-borohydride interactions. Instead, we propose that the small Racah parameter *B* in **4** is a direct consequence of the three-center, two-electron interactions with the borohydride ligands. Depictions of Co−H−B canonical molecular orbitals in **4** (Figure S24) support this view: they show that the metal-BH_3 bonds extend out to encompass the boron atoms, which are located 2.62 Å from cobalt. A metal−carbon or metal−nitrogen interaction of this length would be very weak, but in **4**, the boron is engaged in three-center Co−H−B bonds in which the bridging hydrogen atom lies only 1.75 Å from cobalt. The three-center interaction leads to delocalization of electron density throughout a larger volume than the Co−H bond would on its own, and the expanded metal−ligand bonding orbital allows for reduced electron−electron repulsions.

Another possible consequence of the three-center interaction can be seen in a comparison of the total electron deformation density plots due to the orbital interaction ($\Delta\rho^{orb}$) and Pauli repulsion ($\Delta\rho^{Pauli}$), as derived from the ETS-NOCV analyses. Whereas the total $\Delta\rho^{orb}$ plots show that the metal-alkyl and metal-BH_3 overlaps at the two ends of the BDAM ligand are similar (Figure S22), the total $\Delta\rho^{Pauli}$ plots, which depict the reorganization of electron density due to destabilizing Pauli repulsions in bonding regions between the Co^{3+} and $(BDAM)_3^{3-}$ fragments, show that qualitatively less electron density flows out of metal−ligand bonding regions for Co−B−H interactions than for the Co−C interactions in **4** (Figure 10). The smaller $\Delta\rho^{Pauli}$ isosurface observed for the Co−H−B interactions than for the Co−C interactions is consistent with less electron−electron repulsion at the BH_3 end of the BDAM ligand. A similar phenomenon is not

https://doi.org/10.1021/jacs.3c07336
J. Am. Chem. Soc. 2023, 145, 23585−23599

observed for $Co(CH_3)_3(NH_3)_3$ (Figure S23), evidently because this compound lacks the three-center interactions present in **4**.

To explore whether the B−H bond of a neutral BH_3·L group also has a ligand field strength comparable to that of ammonia, we carried out similar ETS-NOCV analysis on the known compounds $Cr(CO)_5(BH_3NMe_3)$[26] (in which the BH_3NMe_3 group is bound to Cr through a κ^1-BH_3 group) and $Cr(CO)_5(NH_3)$.[86,87] In both compounds (see the Supporting Information for details), the main interaction between the $Cr(CO)_5$ and L fragments is donation into a Cr d orbital of electron density from a B−H bond (for L = BH_3NMe_3) or a N lone pair (for L = NH_3) (Tables S16 and S17). The electron transfer eigenvalues for these L → M interactions are 0.40 and 0.35 for L = BH_3NMe_3 and NH_3, respectively; the net electron transfer from L to Cr (taking into account the small amounts of M → B−H* or N−H* interaction) is 0.21 for L = BH_3NMe_3 and 0.19 for L = NH_3 (Table S18). In addition, the predicted and experimental IR spectra of $Cr(CO)_5(BH_3NMe_3)$[26] and $Cr(CO)_5(NH_3)$[88] in the CO stretching region are very similar (Figure S25).

These findings suggest that even M−H−B interactions in transition metal adducts of neutral boranes are strong field in nature. This somewhat surprising conclusion, which is relevant to B−H bond activation processes, also suggests that agostic σ interactions of C−H bonds with metals may be stronger than previously appreciated.

CONCLUSIONS

Compounds of stoichiometry $M(CH_2NMe_2BH_3)_3$ (M = Ti, Cr, and Co) have been synthesized and characterized. The titanium(III) compound **2** adopts a pseudo-trigonal prismatic geometry, whereas the chromium(III) and cobalt(III) compounds **3** and **4** adopt pseudo-octahedral geometries as is expected for d^1, d^3, and low-spin d^6 metal centers, respectively, in which the ligands are pure σ-donors.[33]

All of the new compounds are fluxional in solution. For pseudo-octahedral **3** and **4**, these fluxional processes include Δ/Λ racemization and bridging/terminal hydride exchange within the borohydride groups. For diamagnetic **4**, the barrier for Δ/Λ racemization is significantly smaller than that for other octahedral cobalt(III) compounds, and a DFT investigation shows that the small barrier could be due to the hemilability of the BH_3 group: a dissociative mechanism (in which a Co−H scission is compensated by another BH_3 group converting from κ^1 to κ^2) has a calculated activation free energy $\Delta G^{\ddagger}$ of 11.8 kcal mol^{-1}. A twist mechanism, however, may also be operative; its computed barrier is $\Delta G^{\ddagger}$ = 14.5 kcal mol^{-1}. It is possible that the barrier for the twist mechanism in **4** is considerably smaller than those seen for other octahedral cobalt(III) complexes because the small steric size of the hydride donors lowers the energy of the sterically more crowded trigonal prismatic transition state.

The ligand field splitting parameters Δ_o measured for **3** and **4** suggest that the ligand field strength of the borohydride end of the BDAM ligand is remarkably high and is similar to that of an alkyl or amine group. In addition, the Racah parameters *B* and *C* for **4** are remarkably small, which suggests that the nephelauxetic effect (i.e., the reduction in electron−electron repulsion) caused by a borohydride group is unusually large. Because the BDAM ligand is a pure σ-donor with no π-accepting character, we propose that the small value of *B* is due to the spatial expansion of the M−H−B three-center bonding orbitals.

The large ligand field strength of the borohydride group in the BDAM ligand is corroborated by the ETS-NOCV analyses of **4** and the model compound $Co(CH_3)_3(NH_3)_3$. The three-center-two-electron bonding of **4** delocalizes the metal d-electrons, and the resulting decrease in electron−electron repulsion is supported by the ETS-NOCV analysis of the electron deformation density plots due to Pauli repulsion. ETS-NOCV analyses of $Cr(CO)_5(BH_3NMe_3)$ and $Cr(CO)_5(NH_3)$ suggest that even B−H bonds of neutral boranes induce ligand field splittings similar to those of ammonia.

These new understandings of the ligand field properties of M−H−B interactions are relevant to the design of borohydride-containing complexes for use in the catalysis, microelectronics, and energy storage industries, as well as to understanding the nature of agostic C−H interactions with metals.

EXPERIMENTAL SECTION

All manipulations were carried out under a vacuum or under argon using standard Schlenk techniques, unless otherwise specified. All glassware was oven-dried before use, and all solvents (pentane, diethyl ether, and thf) were distilled under nitrogen from sodium/benzophenone before use. LiBDAM·thf[30] $CrCl_3(thf)_3$,[89] and $CDFCl_2$,[90] were synthesized by literature procedures. Cobalt(III) acetylacetonate (98%+, Strem) and titanium(IV) chloride (99%, Strem) were used as received. Benzene-d_6 (Cambridge Isotope Laboratories) was distilled from calcium hydride under argon and stored over 3 Å molecular sieves.

Elemental analyses were carried out by the University of Illinois Microanalytical Laboratory. FTIR spectra were acquired on a Thermo Nicolet IR200 spectrometer as mineral oil mulls between KBr plates and processed using the OMNIC software package with automatic baseline corrections. EPR spectra were recorded on a Bruker EMXPlus X-band continuous wave EPR spectrometer at 77 K as frozen solutions in toluene. EPR spectra were simulated and analyzed in Matlab 2022a with the EasySpin 5.2.35 package.[91] UV−visible absorption spectra of **3** were acquired on an Agilent Cary 60 UV−vis spectrophotometer as solutions in diethyl ether; the spectra were deconvoluted to obtain energies for overlapping bands. See elsewhere for details on the collection of UV−visible absorption spectra of **4** using a 10 cm path length cell.[67] The ^1H ^{11}B and $^{11}B\{^1H\}$ NMR data were collected on a Varian Unity Inova 400 instrument at 9.4 T. The room temperature ^{59}Co, $^{13}C\{^1H\}$, and variable-temperature ^1H, $^{13}C\{^1H\}$, and ^{59}Co NMR data were collected on a Varian Unity Inova 600 instrument at 14.1 T. Chemical shifts are reported in δ units (positive shifts to high frequency) relative to $SiMe_4$ (^1H, ^{13}C) by assigning appropriate shifts to solvent peaks or to an external standard of $BF_3{\cdot}Et_2O$ (^{11}B) or $K_3[Co(CN)_6]$ (^{59}Co) by sample replacement. For $Co(CH_2NMe_2BH_3)_3$, ambient temperature $^{13}C\{^1H\}$ NMR data were collected in a 10 mm sample tube; all other NMR data were collected with 5 mm sample tubes. X-ray crystallographic data were collected by the staff of the G. L. Clark X-ray Laboratory at the University of Illinois.

Tris(boranatodimethylaminomethyl)titanium. Ti($CH_2NMe_2BH_3$)$_3$, 2. To a stirred solution of $LiCH_2NMe_2BH_3$·thf (500 mg, 3.18 mmol) in diethyl ether (40 mL) at −78 °C was added dropwise $TiCl_4$ (0.087 mL, 0.795 mmol). The solution was stirred for 1 h at −78 °C and then at 0 °C for an additional 2 h to afford a blue solution and pale-yellow solids. The mixture was dried under vacuum at 0 °C, and the residue was extracted with pentane (40 mL) at 0 °C. The blue extract was filtered, and the filtrate was concentrated to ca. 8 mL and cooled to −20 °C to yield dark blue prisms. Yield: 26 mg (16%). Satisfactory elemental analysis could not be obtained due to the thermal and air sensitivity of **2**. ^1H NMR (C_6D_6, 25 °C, 400.1 MHz): δ 2.46 (s, fwhm = 120 Hz, NMe_2). ^{11}B NMR (C_6D_6, 25 °C,

https://doi.org/10.1021/jacs.3c07336
J. Am. Chem. Soc. 2023, 145, 23585−23599

128.4 MHz): δ −120.9 (s, fwhm = 17,000 Hz, BH_3). IR (cm^{-1}): 2725 vw, 2671 vw, 2374 vs, 2318 s, 2276 s, 2196 m, 2133 m, 2052 sh, 2042 w, 1946 sh, 1807 vw, 1400 w, 1277 m, 1261 sh, 1229 m, 1165 sh, 1152 s, 1120 m, 1076 w, 1045 w, 1006 m, 989 s, 904 m, 855 m, 540 m.

Tris(boranatodimethylaminomethyl)chromium. Cr-($CH_2NMe_2BH_3$)$_3$, 3. To a stirred suspension of $CrCl_3(thf)_3$ (400 mg, 1.06 mmol) in diethyl ether (20 mL) at 0 °C was added dropwise a solution of $LiCH_2NMe_2BH_3$·thf (500 mg, 3.18 mmol) in diethyl ether (20 mL). The resulting mixture was stirred for 1 h at 0 °C, during which time the solution changed from purple to brown. The mixture was warmed to room temperature and stirred for an additional 2 h to afford a red solution. The mixture was filtered, and the filtrate was concentrated to ca. 15 mL and cooled to −20 °C to yield red needles. Two more crops of product could be obtained from the supernatant by concentration and cooling to −20 °C. Yield: 150 mg (53%). Anal. Calcd. for $CrN_3C_9B_3H_{33}$: C, 40.4; H, 12.4; N, 15.7. Found: C, 39.8; H, 12.5; N, 15.3. The C and N analyses are low, probably due to the loss of NMe_3BH_3 by hydrolysis or thermolysis. ^{1}H NMR ($CDFCl_2$, 25 °C, 600.1 MHz): δ −8.27 (s, fwhm = 1000 Hz, NMe_2). IR (cm^{-1}): 2808 w, 2521 s, 2424 vs, 2391 vs, 2373 sh, 2324 s, 2289 m, 2251 m, 2184 m, 2046 vs, 2011 vs, 1832 w, 1730 vw, 1693 vw, 1552 vw, 1469 s, 1462 s, 1448 s, 1410 m, 1276 s, 1265 sh, 1224 s, 1174 s, 1129 s, 1114 s, 1086 vw, 1011 s, 989 s, 920 m, 896 m, 854 m, 721 w, 625 s, 569 m, 469 m, 422 m.

Tris(boranatodimethylaminomethyl)cobalt. Co-($CH_2NMe_2BH_3$)$_3$, 4. To a stirred solution of $Co(acac)_3$ (380 mg, 1.06 mmol) in diethyl ether (20 mL) at 0 °C was added dropwise a solution of $LiCH_2NMe_2BH_3$·thf (500 mg, 3.18 mmol) in diethyl ether (20 mL). The resulting mixture was stirred for 1 h at 0 °C as its color changed from dark green to orange/yellow. The mixture was filtered, and the filtrate was dried under vacuum to afford the crude product (contaminated with some NMe_3BH_3) as an orange-yellow solid in nearly quantitative yield. Analytically pure material can be obtained by sublimation at 66 °C and 1 × 10^{-3} Torr. Sublimation yield: 55 mg (19%). Anal. Calcd. for $CoN_3C_9B_3H_{33}$: C, 39.3; H, 12.1; N, 15.3. Found: C, 39.4; H, 12.1; N, 15.1. ^{1}H NMR (C_6D_6, 25 °C, 400.1 MHz): δ 2.70 (s, 2H, CH_2), 2.29 (s, 6H, NMe_2), −1.11 (q, $^1J_{BH}$ = 96 Hz, 3H, BH_3). $^{13}C\{^1H\}$ NMR (C_7D_8, 25 °C, 150.9 MHz): δ 55.6 (s, NMe_2), 52.7 (br, CH_2). ^{11}B NMR (C_6D_6, 25 °C, 128.4 MHz): δ −11.4 (q, $^1J_{BH}$ = 96 Hz, BH_3). ^{59}Co NMR (C_7D_8, 25 °C, 142.4 MHz): δ 3061 (s, fwhm = 1300 Hz). IR (cm^{-1}): 2427 s, 2390 s, 2333 s, 2293 m, 2239 sh, 2225 w, 2013 s, 1986 sh, 1272 w, 1226 m, 1181 s, 1165 sh, 1136 sh, 1122 m, 996 s, 934 w, 895 w, 858 w. Needles suitable for X-ray diffraction were grown by cooling a saturated diethyl ether solution to −20 °C.

Computational Details. Structural optimizations, single point calculations, frequency calculations, and TD-DFT calculations were performed with the Gaussian 16 program package.[92] The B3LYP[93,94] functional and def2-TZVPP[95] basis set were used for all atoms based on their ability to reproduce experimental parameters and their performance in an agostic M−H−C interaction benchmarking study.[96] GaussSum[97] was used to analyze calculated absorption spectra and obtain orbital contributions in transitions of interest.

Extended-transition-state natural orbitals for chemical valence (ETS-NOCV)[98] were computed using the Multiwfn 3.8 program.[99] Input wavefunction files for individual fragments were generated in Gaussian 16[92] using the B3LYP[93,94] functional and def2-TZVPP[95] basis set. The fragmentation scheme for **2** consists of a singlet Co^{3+} ion and a set of three monoanionic singlet $CH_2NMe_2BH_3^-$ ligands.

■ ASSOCIATED CONTENT

Supporting Information

The Supporting Information is available free of charge at https://pubs.acs.org/doi/10.1021/jacs.3c07336.

Crystallographic studies of compounds **2**, **3**, and **4**; comparisons of their structures with those of previously reported compounds; ^{1}H, $^{13}C\{^1H\}$, ^{11}B, $^{11}B\{^1H\}$, ^{59}Co NMR, IR, and UV−vis spectra of **2**, **3**, and **4**; experimental details of the characterization of the solution phase kinetics of **3** and **4** including Eyring plots for dynamic processes occurring in **4**; VT ^{1}H NMR spectra of **3**; T_1 and T_2* values from VT ^{59}Co NMR inversion recovery experiments of **4**; details of the computational study of **2**; computational study of the dynamic processes occurring in **4**; and ETS-NOCV analyses of **4** and $Co(CH_3)_3(NH_3)_3$ (PDF)

Coordinates of all computationally optimized structures and transition states (TXT)

Accession Codes

CCDC 2265735−2265737 contain the supplementary crystallographic data for this paper. These data can be obtained free of charge via www.ccdc.cam.ac.uk/data_request/cif, or by emailing data_request@ccdc.cam.ac.uk, or by contacting The Cambridge Crystallographic Data Centre, 12 Union Road,-Cambridge CB2 1EZ, UK; fax: +44 1223 336033.

■ AUTHOR INFORMATION

Corresponding Author

Gregory S. Girolami − *School of Chemical Sciences, University of Illinois at Urbana-Champaign, Urbana, Illinois 61801, United States;* orcid.org/0000-0002-7295-1775; Email: girolami@scs.illinois.edu

Authors

R. Joseph Lastowski − *School of Chemical Sciences, University of Illinois at Urbana-Champaign, Urbana, Illinois 61801, United States;* orcid.org/0000-0002-7591-4187

Jonathan T. Yarranton − *Department of Chemistry, Michigan State University, East Lansing, Michigan 48824, United States;* orcid.org/0000-0003-3134-962X

Lingyang Zhu − *School of Chemical Sciences, University of Illinois at Urbana-Champaign, Urbana, Illinois 61801, United States;* orcid.org/0000-0002-6657-271X

Konstantinos D. Vogiatzis − *Department of Chemistry, University of Tennessee, Knoxville, Tennessee 37996, United States;* orcid.org/0000-0002-7439-3850

Complete contact information is available at: https://pubs.acs.org/10.1021/jacs.3c07336

Author Contributions

All authors have given approval to the final version of the manuscript.

Notes

The authors declare no competing financial interest.

■ ACKNOWLEDGMENTS

G.S.G. thanks the National Science Foundation under grant CHE 19-54745 for support of this research and the School of Chemical Sciences of the University of Illinois for computational resources. K.D.V. gratefully acknowledges the National Science Foundation (CHE-1800237) for financial support of this work. We thank Dr. Eric Oldfield and Dr. James McCusker for their helpful discussions.

■ REFERENCES

(1) Marder, T. B.; Lin, Z., Eds. *Contemporary Metal Boron Chemistry I*, 1st ed.; Springer: Berlin, Heidelberg, 2008.

(2) Marks, T. J.; Kolb, J. R. Covalent Transition Metal, Lanthanide, and Actinide Tetrahydroborate Complexes. *Chem. Rev.* **1977**, *77*, 263−293.

(3) Xu, Z.; Lin, Z. Transition Metal Tetrahydroborato Complexes: An Orbital Interaction Analysis of their Structure and Bonding. *Coord. Chem. Rev.* **1996**, *156*, 139−162.
(4) Suárez-Alcántara, K.; Tena García, J. R. Metal Borohydrides Beyond Groups I and II: A Review. *Materials* **2021**, *14*, 2561.
(5) Chakraborty, S.; Dai, H.; Bhattacharya, P.; Fairweather, N. T.; Gibson, M. S.; Krause, J. A.; Guan, H. Iron-Based Catalysts for the Hydrogenation of Esters to Alcohols. *J. Am. Chem. Soc.* **2014**, *136*, 7869−7872.
(6) Zhang, J.; Balaraman, E.; Leitus, G.; Milstein, D. Electron-Rich PNP- and PNN-Type Ruthenium(II) Hydrido Borohydride Pincer Complexes. Synthesis, Structure, and Catalytic Dehydrogenation of Alcohols and Hydrogenation of Esters. *Organometallics* **2011**, *30*, 5716−5724.
(7) Dudle, B.; Blacque, O.; Berke, H. Ethylene Reactions of a $[ReH(\eta^2\text{-}BH_4)(NO)(PPh_3)_2]$ Complex: Reductive Elimination of Ethane and Oxidative Coupling to Butadiene. *Organometallics* **2012**, *31*, 1832−1839.
(8) Sandoval, C. A.; Ohkuma, T.; Muñiz, K.; Noyori, R. Mechanism of Asymmetric Hydrogenation of Ketones Catalyzed by BINAP/1,2-Diamine-Ruthenium(II) Complexes. *J. Am. Chem. Soc.* **2003**, *125*, 13490−13503.
(9) Abelson, J. R.; Girolami, G. S. New Strategies for Conformal, Superconformal, and Ultrasmooth Films by Low Temperature Chemical Vapor Deposition. *J. Vac. Sci. Technol. A* **2020**, *38*, 030802.
(10) Grinderslev, J. B.; Amdisen, M. B.; Skov, L. N.; Møller, K. T.; Kristensen, L. G.; Polanski, M.; Heere, M.; Jensen, T. R. New Perspectives of Functional Metal Borohydrides. *J. Alloys Compd.* **2022**, *896*, 163014.
(11) Nguyen, D. H.; Lauréano, H.; Jugé, S.; Kalck, P.; Daran, J.-C.; Coppel, Y.; Urrutigoity, M.; Gouygou, M. First Dibenzophospholyl-(diphenylphosphino)methane-Borane Hybrid P-$(\eta^2\text{-}BH_3)$ Ligand: Synthesis and Rhodium(I) Complex. *Organometallics* **2009**, *28*, 6288−6292.
(12) Ingleson, M.; Patmore, N. J.; Ruggiero, G. D.; Frost, C. G.; Mahon, M. F.; Willis, M. C.; Weller, A. S. Chelating Monoborane Phosphines: Rational and High-Yield Synthesis of $[(COD)Rh\{(\eta^2\text{-}BH_3)Ph_2PCH_2PPh_2\}]$ $[PF_6]$ (COD = 1,5-cyclooctadiene). *Organometallics* **2001**, *20*, 4434−4436.
(13) Merle, N.; Frost, C. G.; Kociok-Köhn, G.; Willis, M. C.; Weller, A. S. Chelating Phosphane-Boranes as Hemilabile Ligands—Synthesis of $[Mn(CO)_3(\eta^2\text{-}H_3B{\cdot}dppm)]$ $[BAr^{F4}]$ and $[Mn(CO)_4(\eta^1\text{-}H_3B{\cdot}dppm)]$ $[BAr^{F4}]$. *Eur. J. Inorg. Chem.* **2006**, *2006*, 4068−4073.
(14) Merle, N.; Koicok-Köhn, G.; Mahon, M. F.; Frost, C. G.; Ruggerio, G. D.; Weller, A. S.; Willis, M. C. Transition Metal Complexes of the Chelating Phosphine Borane Ligand $Ph_2PCH_2Ph_2P{\cdot}BH_3$. *Dalton Trans.* **2004**, 3883−3892.
(15) Ramalakshmi, R.; Saha, K.; Roy, D. K.; Varghese, B.; Phukan, A. K.; Ghosh, S. New Routes to a Series of σ-Borane/Borate Complexes of Molybdenum and Ruthenium. *Chem.—Eur. J.* **2015**, *21*, 17191−17195.
(16) Iannetelli, A.; Tizzard, G.; Coles, S. J.; Owen, G. R. Sequential Migrations between Boron and Rhodium Centers: A Cooperative Process between Rhodium and a Monosubstituted Borohydride Unit. *Inorg. Chem.* **2018**, *57*, 446−456.
(17) Zafar, M.; Ramalakshmi, R.; Ahmad, A.; Antharjanam, P. K. S.; Bontemps, S.; Sabo-Etienne, S.; Ghosh, S. Cooperative B-H and Si-H Bond Activations by κ^2-N,S-Chelated Ruthenium Borate Complexes. *Inorg. Chem.* **2021**, *60*, 1183−1194.
(18) Pathak, K.; Gayen, S.; Saha, S.; Nandi, C.; Mishra, S.; Ghosh, S. Coordination and Hydroboration of Ru(II)-Borate Complexes: Dihydridoborate vs. Bis(dihydridoborate). *Chem.—Eur. J.* **2022**, *28*, No. e202104393.
(19) van Dijkman, T. F.; de Bruijn, H. M.; Siegler, M. A.; Bouwman, E. Bright Cyan Phosphorescence of a (Phosphane)copper(I) Complex of the Tri-hydrido-pyrazolylborate Ligand $H_3B(3,5\text{-}Ph_2Pz)^-$. *Eur. J. Inorg. Chem.* **2015**, *2015*, 5387−5394.
(20) Dias, H. V. R.; Lu, H.-L. Direct Synthesis of a Bis(pyrazolyl)-boratocopper(I) Complex: Synthesis and Characterization of $[H_2B(3,5\text{-}(CF_3)_2Pz)_2]Cu(PPh_3)_2$ Displaying an Unusual Coordination Mode for a Poly(pyrazolyl)borate Ligand. *Inorg. Chem.* **2000**, *39*, 2246−2248.
(21) Brugos, J.; Cabeza, J. A.; García-Álvarez, P.; Kennedy, A. R.; Pérez-Carreño, E.; Van der Maelen, J. F. 2-(Methylamido)pyridine-Borane: A Tripod κ^3-N,H,H Ligand in Trigonal Bipyramidal Rhodium(I) and Iridium(I) Complexes with an Asymmetric Coordination of Its BH_3 Group. *Inorg. Chem.* **2016**, *55*, 8905−8912.
(22) Oishi, Y.; Albright, T. A.; Fujimoto, H. Fluxionality in $(BH_4)Mn(CO)_4$ and $(BH_4)Cu(PH_3)_2$. *Polyhedron* **1995**, *14*, 2603−2612.
(23) Ariafard, A.; Amini, M. M. Theoretical Study on Interaction of Different Coordination Modes of BH_4 Ligand with Transition Metal in $[TM(BH_4)(CO)_4]^-$ (TM = Cr, Mo). *J. Organomet. Chem.* **2005**, *690*, 84−95.
(24) Wegner, W.; van Leusen, J.; Majewski, J.; Grochala, W.; Kögerler, P. Borohydride as Magnetic Superexchange Pathway in Late Lanthanide Borohydrides. *Eur. J. Inorg. Chem.* **2019**, *2019*, 1776−1783.
(25) Owen, G. R.; Tsoureas, N.; Hope, R. F.; Kuo, Y.-Y.; Haddow, M. F. Synthesis and Characterisation of Group Nine Transition Metal Complexes Containing New Mesityl and Naphthyl Based Azaindole Scorpionate Ligands. *Dalton Trans.* **2011**, *40*, 5906−5915.
(26) Shimoi, M.; Nagai, S.-i.; Ichikawa, M.; Kawano, Y.; Katoh, K.; Uruichi, M.; Ogino, H. Coordination Compounds of Monoborane-Lewis Base Adducts: Syntheses and Structures of $[M(CO)_5(\eta^1\text{-}BH_3{\cdot}L)]$ (M = Cr, Mo, W; L = NMe_3, PMe_3, PPh_3). *J. Am. Chem. Soc.* **1999**, *121*, 11704−11712.
(27) Kiernicki, J. J.; Shanahan, J. P.; Zeller, M.; Szymczak, N. K. Tuning Ligand Field Strength with Pendent Lewis Acids: Access to High Spin Iron Hydrides. *Chem. Sci.* **2019**, *10*, 5539−5545.
(28) Davidson, P. J.; Lappert, M. F.; Pearce, R. Silylmethyl and Related Complexes II. Preparation, Spectra, and Thermolysis of the Tetraneopentyls of Titanium, Zirconium, and Hafnium. *J. Organomet. Chem.* **1973**, *57*, 269−277.
(29) Mowat, W.; Wilkinson, G. Elimination Stabilized Alkyls. Part III. Trimethylsilylmethyl and Neopentyl Alkyls of Transition Metals. *J. Chem. Soc., Dalton Trans.* **1973**, 1120−1124.
(30) Betley, T. A.; Peters, J. C. Synthesis of the (Dialkylamino)-borate, $[Ph_2B(CH_2NMe_2)_2]^-$, Affords Access to N-Chelated Rhodium(I) Zwitterions. *Inorg. Chem.* **2002**, *41*, 6541−6543.
(31) Franz, K.; Fusstetter, H.; Nöth, H. Metallboranate und Boranatometallate. IX; Äther-Addukte von Tris(boranato)-titan(III) und dimere Alkoxy-bis(boranato)-titan(III)-Verbindungen. *Z. Anorg. Allg. Chem.* **1976**, *427*, 97−113.
(32) Jensen, J. A.; Gozum, J. E.; Pollina, D. M.; Girolami, G. S. Titanium, Zirconium, and Hafnium Tetrahydroborates as "Tailored" CVD Precursors for Metal Diboride Thin Films. *J. Am. Chem. Soc.* **1988**, *110*, 1643−1644.
(33) Morse, P. M.; Girolami, G. S. Are d^0 ML_6 Complexes Always Octahedral? The X-ray Structure of Trigonal-prismatic $[Li(tmed)]_2[ZrMe_6]$. *J. Am. Chem. Soc.* **1989**, *111*, 4114−4116.
(34) We cannot completely rule out the possibility that the unusual "$\kappa^{1.5}$" binding mode of two of the borohydride groups in **2** is due to crystallographic disorder between one κ^1 and one κ^2 borohydride group. As previously described for $Ti(BH_4)_3(PR_3)_2$ Goedde, D. M.; Girolami, G. S. Titanium(II) and Titanium(III) Tetrahydroborates. Crystal Structures of $[Li(Et_2O)_2]$ $[Ti_2(BH_4)_5(PMe_2Ph)_4]$, $Ti(BH_4)_3(PMe_2Ph)_2$, and $Ti(BH_4)_3(PEt_3)_2$. *Inorg. Chem.* **2006**, *45*, 1380−1388. this type of disorder between borohydride groups with different binding modes should also be reflected in elongations of thermal ellipsoids for the boron or metal atom. No such elongations, however, are evident in the crystal structure of **2**. In addition, the DFT-optimized geometry of **2** contains two shorter titanium-hydrogen bonds and titanium-boron distances that are in agreement with the experimental structure (Figure S18)
(35) Johnson, A.; Martínez-Martínez, A. J.; Macgregor, S. A.; Weller, A. S. A d^{10} Ag(I) Amine-Borane σ-Complex and Comparison with a

https://doi.org/10.1021/jacs.3c07336
J. Am. Chem. Soc. 2023, 145, 23585−23599

d^8 Rh(I) Analogue: Structures on the η^1 to η^2:η^2 Continuum. *Dalton Trans.* **2019**, *48*, 9776−9781.
(36) Daly, S. R.; Kim, D. Y.; Girolami, G. S. Lanthanide *N,N*-Dimethylaminodiboranates as a New Class of Highly Volatile Chemical Vapor Deposition Precursors. *Inorg. Chem.* **2012**, *51*, 7050−7065.
(37) Jensen, J. A.; Girolami, G. S. Synthesis, Characterization, and X-ray Crystal Structures of the Divalent Titanium Complex Ti(η^2-BH_4)$_2$(dmpe)$_2$ and the Unidentate Tetrahydroborate Complex V(η^1-BH_4)$_2$(dmpe)$_2$. *Inorg. Chem.* **1989**, *28*, 2107−2113.
(38) Marks, T. J.; Kennelly, W. J. Bis(η^5-cyclopentadienyl)vanadium Tetrahydroborate. Covalent Organotransition Metal Borohydride with Unusual Spectroscopic and Dynamic Properties. *J. Am. Chem. Soc.* **1975**, *97*, 1439−1443.
(39) Dunbar, A. C.; Girolami, G. S. Synthesis and Characterization of Calcium *N,N*-Dimethylaminodiboranates as Possible Chemical Vapor Deposition Precursors. *Inorg. Chem.* **2014**, *53*, 888−896.
(40) Kim, D. Y.; Girolami, G. S. Highly Volatile Magnesium Complexes with the Aminodiboranate Anion, a New Chelating Borohydride. Synthesis and Characterization of Mg($H_3BNMe_2BH_3$)$_2$ and Related Compounds. *Inorg. Chem.* **2010**, *49*, 4942−4948.
(41) Makhaev, V. D. Structural and Dynamic Properties of Tetrahydroborate Complexes. *Russ. Chem. Rev.* **2000**, *69*, 727−746.
(42) Van Doorslaer, S.; Shane, J. J.; Stoll, S.; Schweiger, A.; Kranenburg, M.; Meier, R. J. Continuous Wave and Pulse EPR as a Tool for the Characterization of Monocyclopentadienyl Ti(III) Catalysts. *J. Organomet. Chem.* **2001**, *634*, 185−192.
(43) Horáček, M.; Kupfer, V.; Thewalt, U.; Polášek, M.; Mach, K. Synthesis and Structures of Paramagnetic Binuclear (η^8-1,4-bis(trimethylsilyl)cyclooctatetraenide)titanium(III) Chlorides. *J. Organomet. Chem.* **1999**, *579*, 126−132.
(44) Maurelli, S.; Morra, E.; Van Doorslaer, S.; Busico, V.; Chiesa, M. EPR Investigation of $TiCl_3$ Dissolved in Polar Solvents—Implications for the Understanding of Active Ti(III) Species in Heterogeneous Ziegler-Natta Catalysts. *Phys. Chem. Chem. Phys.* **2014**, *16*, 19625−19633.
(45) Shaham, N.; Cohen, H.; Meyerstein, D.; Bill, E. EPR Measurements Corroborate Information Concerning the Nature of $(H_2O)_5Cr^{III}$-alkyl Complexes. *J. Chem. Soc., Dalton Trans.* **2000**, 3082−3085.
(46) Reich, H. J. WinDNMR: Dynamic NMR Spectra for Windows. *J. Chem. Educ.* **1995**, *72*, 1086.
(47) It is possible that a temperature-dependent quadrupolar broadening of the BH_3 ^{1}H NMR resonances (similar to that seen for the cobalt-bound CH_2 group, see the Supporting Information) adds additional error to the fitted spectral line shapes. However, the high degree of linearity in the Eyring plot of the BH_3 rotational rates (Figure S12, R = 0.999) suggests this effect is not significant.
(48) Evans, J.; Johnson, B. F. G.; Lewis, J.; Matheson, T. W.; Norton, J. R. Carbon-13 Nuclear Magnetic Resonance Spectra of Polynuclear Carbonyls of Cobalt and Rhodium. *J. Chem. Soc., Dalton Trans.* **1978**, 626−634.
(49) Aime, S.; Milone, L.; Osella, D.; Poli, A. Solution Structures and Dynamics of $Co_4(CO)_{12}$ and $HFeCo_3(CO)_{12-x}L_x$ (x = 0−3; L = Group V Ligand). *Inorg. Chim. Acta* **1978**, *30*, 45−49.
(50) Plečnik, C. E.; Liu, S.; Chen, X.; Meyers, E. A.; Shore, S. G. Lanthanide-Transition-Metal Carbonyl Complexes: New $[Co_4(CO)_{11}]^{2-}$ Clusters and Lanthanide(II) Isocarbonyl Polymeric Arrays. *J. Am. Chem. Soc.* **2004**, *126*, 204−213.
(51) Todd, L. J.; Wilkinson, J. R. A ^{13}C NMR of Metal Carbonyl Derivative having Quadrupolar Nuclei (Mn, Co, Re and Ir). *J. Organomet. Chem.* **1974**, *80*, C31−C34.
(52) Kawano, Y.; Kakizawa, T.; Yamaguchi, K.; Shimoi, M. A Computational Study on Fluxional Behavior of Group 6 and 7 Transition-metal Complexes of Borane-Lewis Base Adducts. *Chem. Lett.* **2006**, *35*, 568−569.
(53) Eaton, S. S.; Hutchison, J. R.; Holm, R. H.; Muetterties, E. L. Intramolecular Rearrangement Reactions of Tris-Chelate Complexes. III. Analysis of the Rearrangements of Tris(α-isopropenyl and α-isopropyltropolonato)aluminum(III) and -cobalt(III). Examples of Stereochemically Nonrigid Aluminum(III) and Cobalt(III) Complexes. *J. Am. Chem. Soc.* **1972**, *94*, 6411−6426.
(54) Fay, R. C.; Piper, T. S. Coordination Compounds of Trivalent Metals with Unsymmetrical 1,3-Diketones. III. Mechanism of Stereochemical Rearrangements. *Inorg. Chem.* **1964**, *3*, 348−356.
(55) Palazzotto, M. C.; Duffy, D. J.; Edgar, B. L.; Que, L.; Pignolet, L. H. Dynamic Stereochemistry of Tris(chelate) Complexes. I. Tris(dithiocarbamato) Complexes of Iron, Cobalt, and Rhodium. *J. Am. Chem. Soc.* **1973**, *95*, 4537−4545.
(56) Fay, R. C.; Girgis, A. Y.; Klabunde, U. Rearrangements of Metal Tris(β-diketonates). I. Partial Resolution and Racemization of Some Tris(acetylacetonates). *J. Am. Chem. Soc.* **1970**, *92*, 7056−7060.
(57) Gaydon, Q.; Bohle, D. S. Separation of Isomers and Mechanisms of Inversion of Stereochemistry of Group 9 d^6 Tris-Chelate Complexes of Hinokitiol. *Inorg. Chem.* **2021**, *60*, 13567−13577.
(58) Gaydon, Q.; Bohle, D. S. Coordination Chemistry of the Parent Dithiocarbamate $H_2NCS_2^-$: Organometallic Chemistry and Tris-Chelates of Group 9 Metals. *Inorg. Chem.* **2022**, *61*, 4660−4672.
(59) For nondissociative racemizations of tris(chelate) metal complexes, correlations have been drawn between the racemization mechanism (i.e., whether it is a Bailar or a Ray-Dutt twist) and certain molecular geometric parameters such as ligand bite angle, normalized bite (b), compression ratio (s/h), pitch angle (ψ), and face twist angle (ϕ). All these parameters describe the degree to which the first coordination sphere of a metal center is distorted away from idealized octahedral geometry toward trigonal prismatic geometry.[58] See also (a) Rzepa, H. S.; Cass, M. E. In Search of the Bailar and Rây-Dutt Twist Mechanisms That Racemize Chiral Trischelates: A Computational Study of Sc^{III}, Ti^{IV}, Co^{III}, Zn^{II}, Ga^{III}, and Ge^{IV} Complexes of a Ligand Analogue of Acetylacetonate. *Inorg. Chem.* **2007**, *46*, 8024−8031. (b) Davis, A. V.; Firman, T. K.; Hay, B. P.; Raymond, K. N. d-Orbital Effects on Stereochemical Non-Rigidity: Twisted Ti^{IV} Intramolecular Dynamics. *J. Am. Chem. Soc.* **2006**, *128*, 9484−9496. Many of these geometric parameters, however, are not particularly useful for the current compounds because they assume that there is a single metal-ligand distance (i.e., that the ligand is symmetric), whereas in compounds **2**−**4** the M−C and M−H bonds to the two ends of the BDAM ligand have very different lengths. Most useful for our purposes is the face twist angle (the torsional angle between the triangle formed by the metal-bound carbon atoms and the triangle formed by the metal-hydrogen atoms), which for an ideal octahedron and a trigonal prism has a value of 60 and 0°, respectively
(60) The absence of any NMR resonances attributable to a *mer* isomer of **4** in the VT ^{1}H and ^{13}C{^{1}H} NMR data (Figures 4 and 5) suggests that the Ray-Dutt mechanism is not occurring. The mer isomer of **4** may be energetically disfavored because some alkyl groups would be mutually trans and some B−H groups would also be mutually trans.
(61) Edelson, M. R.; Plane, R. A. The Photochemical Aquation of $Cr(NH_3)_6^{+3}$ and $Cr(NH_3)_5H_2O^{+3}$. *J. Phys. Chem.* **1959**, *63*, 327−330.
(62) Alexander, J. J.; Gray, H. B. Electronic Structures of Hexacyanometalate Complexes. *J. Am. Chem. Soc.* **1968**, *90*, 4260−4271.
(63) Dunken, H.; Marx, G. Ligandenfeldparameter von Cr-$(CH_3)_6$(Li Dioxan)$_3$. *Z. Chem.* **1966**, *6*, 436−437.
(64) Ballhausen, C. J. *Introduction to Ligand Field Theory*; McGraw-Hill Book Company, 1962; pp 226−273.
(65) Figgis, B. N.; Hitchman, M. A. *Ligand Field Theory and Its Applications*; Wiley VCH, 2000; pp 179−227.
(66) Thomson, J.; Baird, M. C. Trends in the Spectrochemical Series and ^{31}P Chemical Shifts of Five-coordinated Cyclopentadienylnickel(II) Complexes^{31}P Chemical Shifts of Five-coordinated Cyclopentadienylnickel(II) Complexes. *Can. J. Chem.* **1973**, *51*, 1179−1182.
(67) Yarranton, J. T.; McCusker, J. K. Ligand-Field Spectroscopy of Co(III) Complexes and the Development of a Spectrochemical Series

https://doi.org/10.1021/jacs.3c07336
J. Am. Chem. Soc. 2023, 145, 23585−23599

for Low-Spin d^6 Charge-Transfer Chromophores. *J. Am. Chem. Soc.* **2022**, *144*, 12488−12500.
(68) Shao, Y. C.; Karki, B.; Huang, W.; Feng, X.; Sumanasekera, G.; Guo, J. H.; Chuang, Y. D.; Freelon, B. Spectroscopic Determination of Key Energy Scales for the Base Hamiltonian of Chromium Trihalides. *J. Phys. Chem. Lett.* **2021**, *12*, 724−731.
(69) Okumura, K. Paramagnetic Resonance of Diluted $[Cr(NH_3)_6]$-Cl_3. *J. Phys. Soc. Jpn.* **1962**, *17*, 1341−1358.
(70) Berben, L. A.; Long, J. R. Homoleptic Trimethylsilylacetylide Complexes of Chromium(III), Iron(II), and Cobalt(III): Syntheses, Structures, and Ligand Field Parameters. *Inorg. Chem.* **2005**, *44*, 8459−8468.
(71) Lindley, B. M.; Wolczanski, P. T.; Cundari, T. R.; Lobkovsky, E. B. First-Row Transition Metal and Lithium Pyridine-ene-amide Complexes Exhibiting N- and C-Isomers and Ligand-Based Activation of Benzylic C-H Bonds. *Organometallics* **2015**, *34*, 4656−4668.
(72) Wentworth, R. A. D.; Piper, T. S. A Crystal Field Model for the Spectral Relationships in Monoacidopentaammine and Diacdote-traammine Complexes of Cobalt(III). *Inorg. Chem.* **1965**, *4*, 709−714.
(73) We note that values of Δ_o, *B*, and *C* for low-spin d^6 metal complexes are commonly derived from the observed transition energies by a second method that involves approximating the determinant using only the diagonal terms and solving a series of linearly independent equations.[67] The resulting values are easier to derive from the observed spectrum, but afford less accurate information about the true electronic properties of the ligands. Adopting this approach for **4** affords values of 27,250, 360, and 4630 cm^{-1} for the parameters Δ_o, *B*, and *C*, respectively; notably, the d-orbital splitting Δ_o is even larger than the value obtained by the full-matrix diagonalization approach.
(74) Bendix, J. *LIGFIELD, 092*: Copenhagen, Denmark, 1993.
(75) Wylezich, T.; Sontakke, A. D.; Castaing, V.; Suta, M.; Viana, B.; Meijerink, A.; Kunkel, N. One Ion, Many Facets: Efficient, Structurally and Thermally Sensitive Luminescence of Eu^{2+} in Binary and Ternary Strontium Borohydride Chlorides. *Chem. Mater.* **2019**, *31*, 8957−8968.
(76) Paskevicius, M.; Jepsen, L. H.; Schouwink, P.; Černý, R.; Ravnsbæk, D. B.; Filinchuk, Y.; Dornheim, M.; Besenbacher, F.; Jensen, T. R. Metal Borohydrides and Derivatives—Synthesis, Structure and Properties. *Chem. Soc. Rev.* **2017**, *46*, 1565−1634.
(77) Khalimon, A. Y.; Holland, J. P.; Kowalczyk, R. M.; McInnes, E. J. L.; Green, J. C.; Mountford, P.; Nikonov, G. I. Synthesis and Molecular and Electronic Structure of an Unusual Paramagnetic Borohydride Complex $Mo(NAr)_2(PMe_3)_2(\eta^2\text{-}BH_4)$. *Inorg. Chem.* **2008**, *47*, 999−1006.
(78) Stockmayer, W. H.; Rice, D. W.; Stephenson, C. C. Thermodynamic Properties of Sodium Borohydride and Aqueous Borohydride Ion. *J. Am. Chem. Soc.* **1955**, *77*, 1980−1983.
(79) Pantazis, D. A.; McGrady, J. E.; Besora, M.; Maseras, F.; Etienne, M. On the Origin of α- and β-Agostic Distortions in Early-Transition-Metal Alkyl Complexes. *Organometallics* **2008**, *27*, 1128−1134.
(80) Haaland, A.; Scherer, W.; Ruud, K.; McGrady, G. S.; Downs, A. J.; Swang, O. On the Nature and Incidence of β-Agostic Interactions in Ethyl Derivatives of Early Transition Metals: Ethyltitanium Trichloride and Related Compounds. *J. Am. Chem. Soc.* **1998**, *120*, 3762−3772.
(81) Mitoraj, M. P.; Michalak, A.; Ziegler, T. On the Nature of the Agostic Bond between Metal Centers and β-Hydrogen Atoms in Alkyl Complexes. An Analysis Based on the Extended Transition State Method and the Natural Orbitals for Chemical Valence Scheme (ETS-NOCV). *Organometallics* **2009**, *28*, 3727−3733.
(82) von Frantzius, G.; Streubel, R.; Brandhorst, K.; Grunenberg, J. How Strong Is an Agostic Bond? Direct Assessment of Agostic Interactions Using the Generalized Compliance Matrix. *Organometallics* **2006**, *25*, 118−121.
(83) MacInnis, M. C.; DeMott, J. C.; Zolnhofer, E. M.; Zhou, J.; Meyer, K.; Hughes, R. P.; Ozerov, O. V. Cationic Two-Coordinate Complexes of Pd(I) and Pt(I) Have Longer Metal-Ligand Bonds Than Their Neutral Counterparts. *Chem.* **2016**, *1*, 902−920.
(84) Jerabek, P.; Schwerdtfeger, P.; Frenking, G. Dative and Electron-sharing Bonding in Transition Metal Compounds. *J. Comput. Chem.* **2019**, *40*, 247−264.
(85) Liu, S.; Smith, B. A.; Kirkland, J. K.; Vogiatzis, K. D.; Girolami, G. S. Nature of the Short Rh-Li Contact between Lithium and the Rhodium ω-Alkenyl Complex $[Rh(CH_2CMe_2CH_2CH{=}CH_2)_2]^-$. *Inorg. Chem.* **2021**, *60*, 8790−8801.
(86) Behrens, H.; Harder, N. Zur Kenntnis der Chemie der Metallcarbonyle in Flüssigem Ammoniak, XII. Die Reaktionen der Hexacarbonyle der Chromgruppe und ihrer Bipyridyl-(2,2′)- und 1,10-Phenanthrolin-Substitutionsprodukte im Ammonosystem. *Chem. Ber.* **1964**, *97*, 433−442.
(87) Strohmeier, W.; Guttenberger, J. F.; Blumenthal, H.; Albert, G. Thermische und Photochemische Reaktion von Aliphatischen Aminen mit Metallhexacarbonylen. *Chem. Ber.* **1966**, *99*, 3419−3424.
(88) Fischer, E. O.; Bathelt, W.; Müller, J. Stibin-pentacarbonyl-Komplexe von Chrom(0), Molybdän(0) und Wolfram(0). *Chem. Ber.* **1971**, *104*, 986−992.
(89) So, J. H.; Boudjouk, P. A Convenient Synthesis of Solvated and Unsolvated Anhydrous Metal Chlorides via Dehydration of Metal Chloride Hydrates with Trimethylchlorosilane. *Inorg. Chem.* **1990**, *29*, 1592−1593.
(90) Siegel, J. S.; Anet, F. A. L. Dichlorofluoromethane-d: A Versatile Solvent for VT-NMR Experiments. *J. Org. Chem.* **1988**, *53*, 2629−2630.
(91) Stoll, S.; Schweiger, A. EasySpin, a Comprehensive Software Package for Spectral Simulation and Analysis in EPR. *J. Magn. Reson.* **2006**, *178*, 42−55.
(92) Frisch, M. J.; Trucks, G. W.; Schlegel, H. B.; Scuseria, G. E.; Robb, M. A.; Cheeseman, J. R.; Scalmani, G.; Barone, V.; Petersson, G. A.; Nakatsuji, H.; Li, X.; Caricato, M.; Marenich, A. V.; Bloino, J.; Janesko, B. G.; Gomperts, R.; Mennucci, B.; Hratchian, H. P.; Ortiz, J. V.; Izmaylov, A. F.; Sonnenberg, J. L.; Williams; Ding, F.; Lipparini, F.; Egidi, F.; Goings, J.; Peng, B.; Petrone, A.; Henderson, T.; Ranasinghe, D.; Zakrzewski, V. G.; Gao, J.; Rega, N.; Zheng, G.; Liang, W.; Hada, M.; Ehara, M.; Toyota, K.; Fukuda, R.; Hasegawa, J.; Ishida, M.; Nakajima, T.; Honda, Y.; Kitao, O.; Nakai, H.; Vreven, T.; Throssell, K.; Montgomery, J. A., Jr.; Peralta, J. E.; Ogliaro, F.; Bearpark, M. J.; Heyd, J. J.; Brothers, E. N.; Kudin, K. N.; Staroverov, V. N.; Keith, T. A.; Kobayashi, R.; Normand, J.; Raghavachari, K.; Rendell, A. P.; Burant, J. C.; Iyengar, S. S.; Tomasi, J.; Cossi, M.; Millam, J. M.; Klene, M.; Adamo, C.; Cammi, R.; Ochterski, J. W.; Martin, R. L.; Morokuma, K.; Farkas, O.; Foresman, J. B.; Fox, D. J. *Gaussian 16*. Rev. C.01: Wallingford, CT, 2016;.
(93) Becke, A. D. Density-Functional Thermochemistry. III. The Role of Exact Exchange. *J. Chem. Phys.* **1993**, *98*, 5648−5652.
(94) Lee, C.; Yang, W.; Parr, R. G. Development of the Colle-Salvetti Correlation-energy Formula into a Functional of the Electron Density. *Phys. Rev. B* **1988**, *37*, 785−789.
(95) Weigend, F.; Ahlrichs, R. Balanced Basis Sets of Split Valence, Triple Zeta Valence and Quadruple Zeta Valence Quality for H to Rn: Design and Assessment of Accuracy. *Phys. Chem. Chem. Phys.* **2005**, *7*, 3297−3305.
(96) Flener-Lovitt, C.; Woon, D. E.; Dunning, T. H.; Girolami, G. S. A DFT and ab Initio Benchmarking Study of Metal-Alkane Interactions and the Activation of Carbon-Hydrogen Bonds. *J. Phys. Chem. A* **2010**, *114*, 1843−1851.
(97) O'boyle, N. M.; Tenderholt, A. L.; Langner, K. M. cclib: A Library for Package-independent Computational Chemistry Algorithms. *J. Comput. Chem.* **2008**, *29*, 839−845.
(98) Mitoraj, M.; Michalak, A. Natural Orbitals for Chemical Valence as Descriptors of Chemical Bonding in Transition Metal Complexes. *J. Mol. Model.* **2007**, *13*, 347−355.
(99) Lu, T.; Chen, F. Multiwfn: A Multifunctional Wavefunction Analyzer. *J. Comput. Chem.* **2012**, *33*, 580−592.

https://doi.org/10.1021/jacs.3c07336
J. Am. Chem. Soc. 2023, 145, 23585−23599